ABSTRACT

Title of Dissertation / Thesis: SMALL ANGLE NEUTRON SCATTERING OF ARBORESCENT GRAFT POLYMER SOLUTIONS

Kai-Chi Lai, Master of Science, 2004

Dissertation / Thesis Directed By: Professor and Chair, Robert M. Briber, Department of Materials of Science and Engineering

Arborescent graft polymers (AGP) are branched macromolecules resulting from successive cycles of random functionalization and subsequent end-grafting of anionic polymerized chains to form a highly branched polymer molecule. Small Angle Neutron Scattering (SANS) was used to characterize the size and shape of generation 3 and generation 4 polystyrene (PS) based arborescent graft polymers where the final generation of the polymer molecule composed of deuterated PS. Contrast variation techniques were used to match the solvent to the either the PS core or the deuterated PS shell. A core-shell model was used to fit the SANS data with good success but the contrast of the core and shell were found to deviate from that of pure PS and deuterated PS respectively leading to the conclusion that there is some phase mixing between the final generation and the substrate (i.e. previous generation). This is consistent with the random functionalization of the substrate prior to end-grafting on the final generation. Density profiles of generation 4 and generation 3 arborescent graft polymers in different solvents are calculated, and the size of the

molecule is found to be dominated by the solvent quality. Even though the scattering data for molecules dissolved in shell-match solvent can be well fitted, physical interpretation is poor. A sphere model were used to fit the scattering and the result was not good The relation between radius of gyration and hydrodynamic radius is also discussed. The radius of gyration is found to be determined by the scattering length density of core and shell, core radius and total hydrodynamic radius. The radius of gyration from Guinier plot is discussed and found to be unreliable due to non-uniform density distribution of the molecule.

SMALL ANGLE NEUTRON SCATTERING OF ARBORESCENT GRAFT POLYMER SOLUTIONS

By

Kai-Chi Lai

Thesis or Dissertation submitted to the Faculty of the Graduate School of the
University of Maryland, College Park, in partial fulfillment
of the requirements for the degree of
Master of Science
2004

Advisory Committee:
Professor Robert M. Briber, Chair
Associate Professor Peter Kofinas
Associate Professor Luz Martinez-Miranda

DEDICATION

To my parents, my brothers, and my fiancée, Wen-Ting

for their ceaseless encouraging and support.

ACKNOWLEDGEMENT

I would like to extend my sincere gratitude and appreciation to many people who made this master thesis possible. I am highly indebted to my advisor Professor Robert M. Briber who has been very patient and very brilliant. Special thanks are due to Dr. Gauthier at Department of Chemistry, Institute for Polymer Research, University of Waterloo, Canada, who synthesized arborescent graft polymers and provided lots of information. Special thanks are to Dr. Seok-Il Yun at Condensed Matter Sciences Division, Oak Ridge National Laboratory who has instructed me in the fitting process.

Many thanks go to Center for Neutron Research of the National Institute of Standards and Technology National Institute Standard & Technology, Gaithersburg, whose assistance was vital for the research. These include Dr. Derek Ho, Dr. John Barker, Dr. Lionel Porcar, and Dr. Steve Kline.

I would also like to acknowledge all the group members, Zhaoliang Lin, Hongxia Feng who directed and assisted me in the SANS experiment, Xing Zhang who provides the information in the lab and software support, and Nicolae Albu who is a good company.

Finally, to my dear families, who always give me the best support. Special thanks to my fiancée, Wen-Ting who stayed with me and gave me great assistance in the last month. I love you all.

TABLE OF CONTENTS

LIST OF TABLES

LIST OF FIGURES

Chapter 1

Introduction

The molecular architecture significantly affects physical properties of polymers. In this chapter the chain architecture of polymers will be discussed in relation to small-angle neutron scattering (SANS) and other methods for measuring the chain architecture will be reviewed.

1.1 Chain Architecture

Polymers are macromolecules made up of small molecules linked together by covalent bonds [1-3]. The small molecules that react together to form the polymer chain are termed monomers, and the reaction is called polymerization. The number of monomers in a given polymer chain is called the degree of polymerization. The polymers can differ not only in the arrangement of the bonding, monomer chemistry and sequence but also in terms of their chain architecture. The chain architecture is related to spatial arrangement of the monomers which is determined by the type of bonding. Polymers can be classified as linear, branched, or crosslinked based on their

architecture as shown in figure 1-1.

1.1.1 Branched Polymers

Branched polymers have sections of polymer chain which are joined to the main chain at branch points, and are characterized in terms of the number and size of the branches. Special classes of branched polymers which have controlled architectures such as dendrimers, hyperbranched polymers, and arborescent graft polymers have been developed in recent years [4-7, 8-17].

1.1.1.1 Dendrimer

Dendrimers are branched polymers which consist of monomers that emanate from a central core as shown in figure 1-2 (a) [4, 5, 8-10, 18]. They are often synthesized by stepwise repetitive reactions with each subsequent growth step, branching and creating new "generation" of polymer. Dendrimers have regular shape, narrow molecular weight distribution, and can have functional terminal end groups. These new polymers were first synthesized in early 1980's independently by Tomalia and Newkome, and called dendrimers to describe their tree-like branching structure [9]. Current research on dendrimers is targeted at finding useful industrial applications.

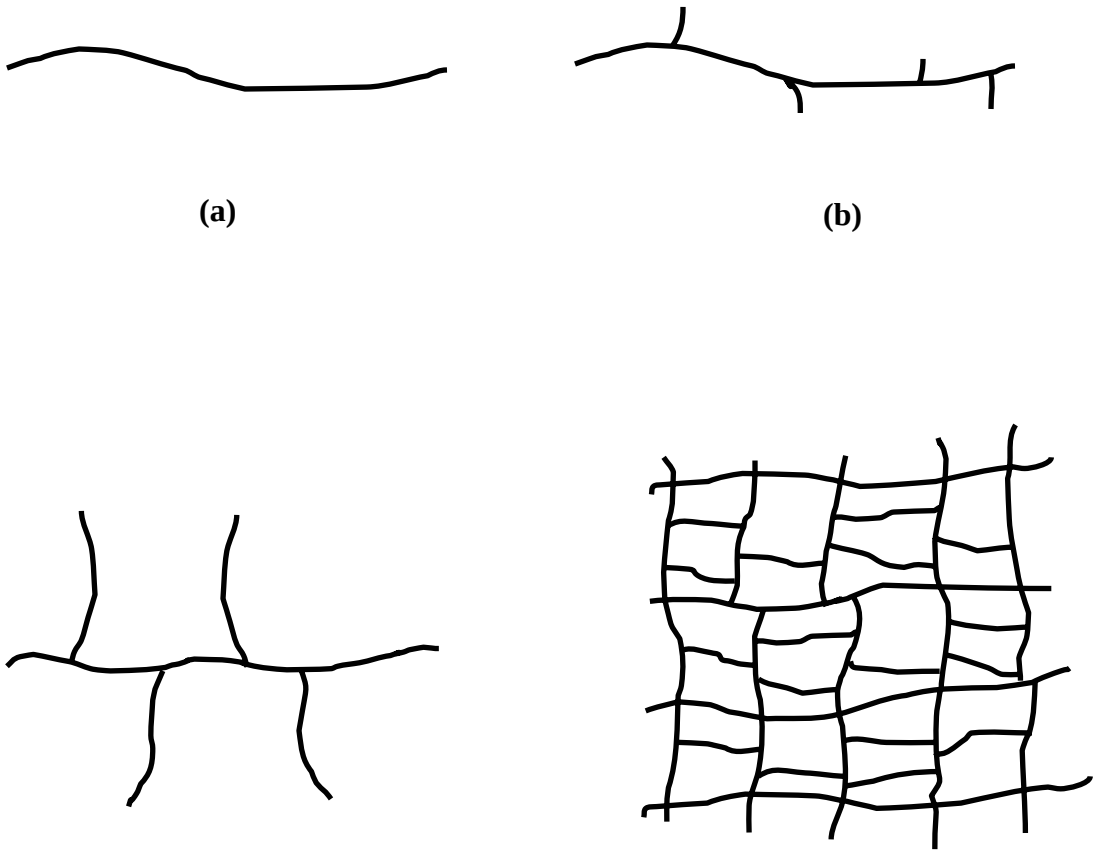

Figure 1-1 Schematic representation of polymers (a) linear polymer, (b) short chain branched polymer, (c) long chain branched polymer, (d) crosslinked polymer.

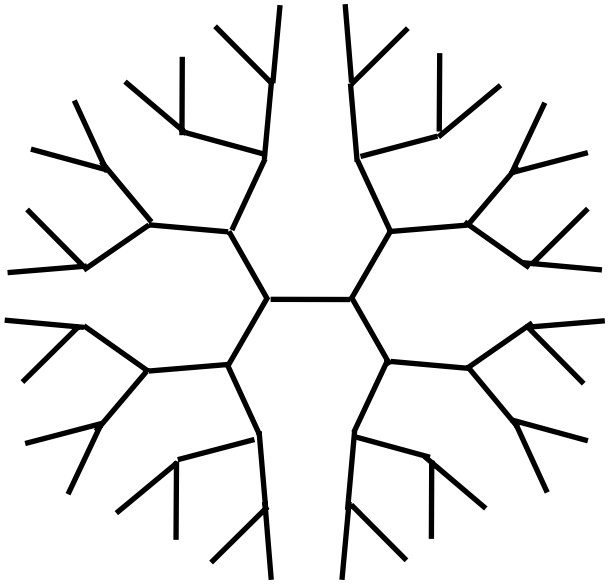

(a)

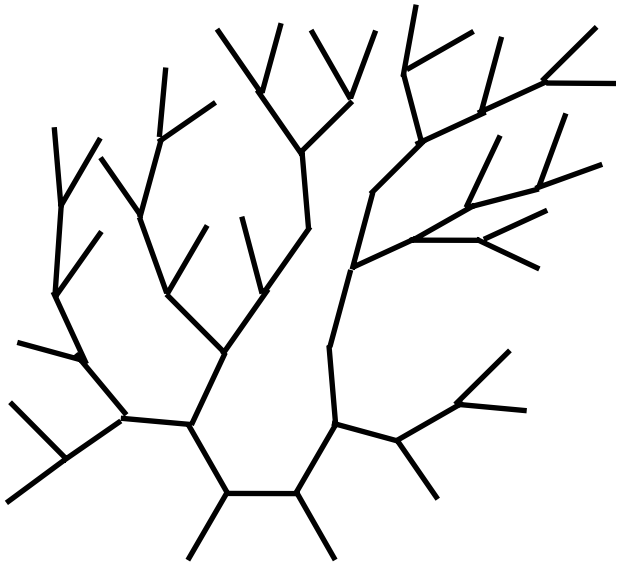

(b)

Figure 1-2 Schematic representation of branched polymers: (a)dendrimer, (b) hyperbranched polymer.

They can be used as polymer crosslinkers, sensors, catalysts, size standard, and drug release systems due to interior void volume [10, 19, 20].

1.1.1.2 Hyperbranched Polymers

Hyperbranched polymers are usually synthesized in a single step by polycondensation [6, 11]. Hyperbranched polymers are highly branched, but unlike dendrimers, these polymers have a largely irregular shape and are not highly symmetrical as shown in figure 1-1 (b) [18]. Since not every repeat unit contains a branch point, they are polydisperse and have a broad molecular weight distribution in comparison with dendrimers.

1.1.1.3 Arborescent Graft Polymers

Arborescent graft polymers are branched macromolecules synthesized by successive cycles of functionalization and grafting reactions [7, 12-17, 21, 22, 23]. Grafting linear polystyryl anions onto a partially acetylated linear polystyrene yields a generation 0 polymer as shown in figure 1-3 [7, 12, 13]. By repetition of the acetylation and anionic grafting reactions, higher generation polymers are synthesized. The grafting sites are believed to be distributed randomly throughout the molecule

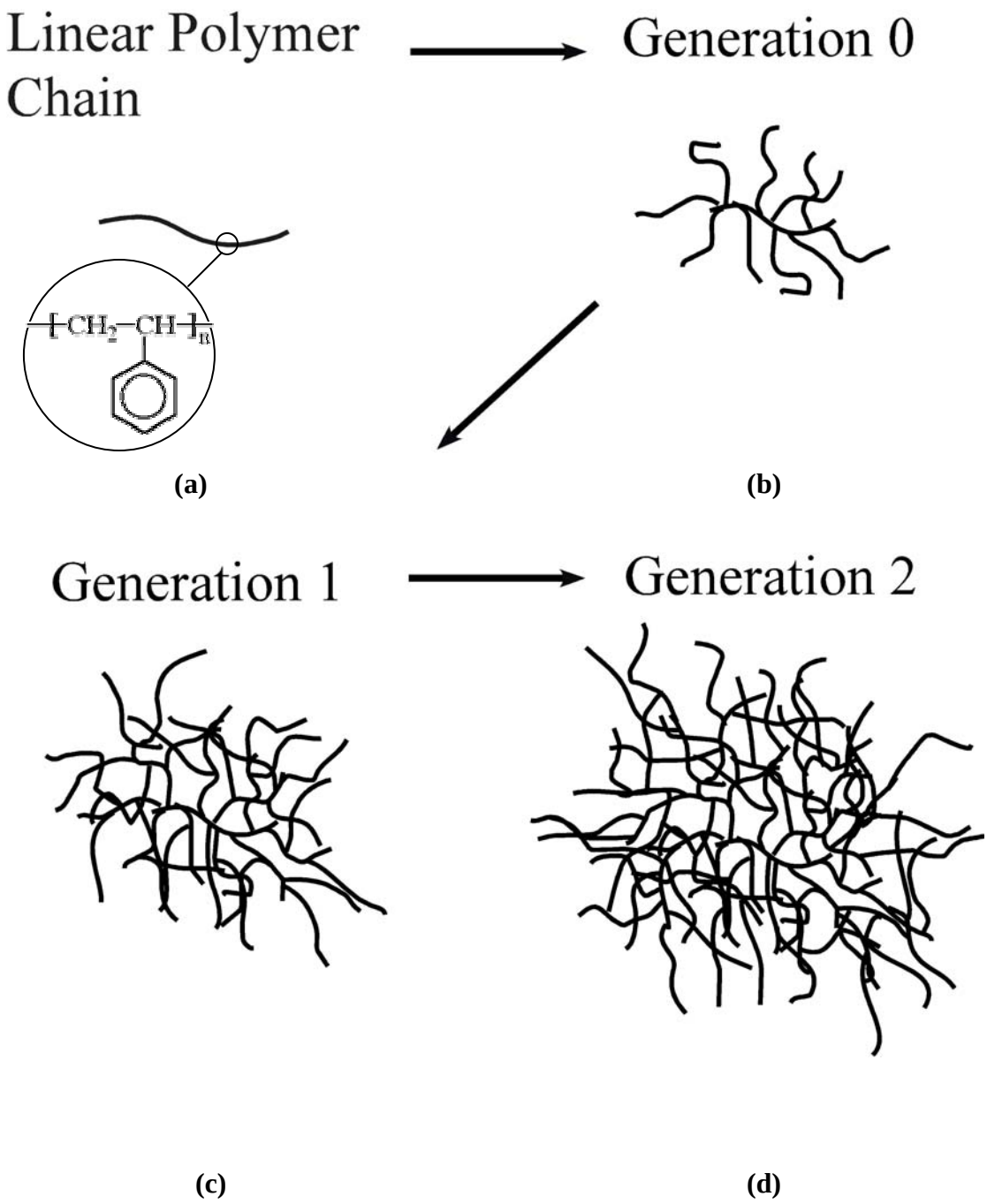

Figure 1-3 Schematic representation of branched polymer: arborescent graft polymer.

[12]. The structure of arborescent graft polymers is related to dendrimer molecules, but since the building blocks are polymer chains rather than monomers, arborescent graft polymers with very high molecular weight can be achieved within a few generations [12]. In addition, the grafting reaction in arborescent polymer molecules occurs randomly, as opposed to dendrimer molecules where the branching occurs at regular intervals throughout the structure. Since the branching in arborescent polymers is very dense, the distribution of graft sites becomes uniform throughout the molecule. The arborescent polymers should show spherical symmetry when the initial backbone molecular mass is comparable to the side chain molecular mass. An interesting characteristic of these systems is the possibility to synthesize well defined macromolecules with a wide range of molecular mass and controlled shapes such as spheres, ellipsoids, and rods by varying the branching density and/or the molecular weight of the initial backbone and/or the side chains.

1.2 Small-Angle Neutron Scattering

In general, scattering means a change in momentum for the radiation beam (x-ray, neutron, light, etc) from its incident value due to interaction with the molecules in a sample. If the radiation beam does not exchange energy with the

molecules and only its direction changes in the scattering event, the scattering is known as elastic scattering. Consequently the magnitude of the incident wave vector $\mathbf{k_i}$ is the same as that of the scattered wave vector $\mathbf{k_s}$ as shown in figure 1-4**.** The q, the magnitude of the scattering wave vector is defined as

$$q = |\mathbf{q}| = |\mathbf{k}_i - \mathbf{k}_s| = \frac{4\pi}{\lambda}\sin\theta \qquad (1.1)$$

The angular distribution of the scattered intensity I(q) represents the structure of the sample. Bragg's law is well known as

$$n\lambda = 2d\sin\theta \qquad (1.2)$$

Combining eq. (1.1) and (1.2) yields

$$d = \frac{2\pi}{q} \qquad (1.3)$$

Therefore, data at lower q presents probe longer length scale.

Neutrons are one kind of the radiation that can be used as scattering source.

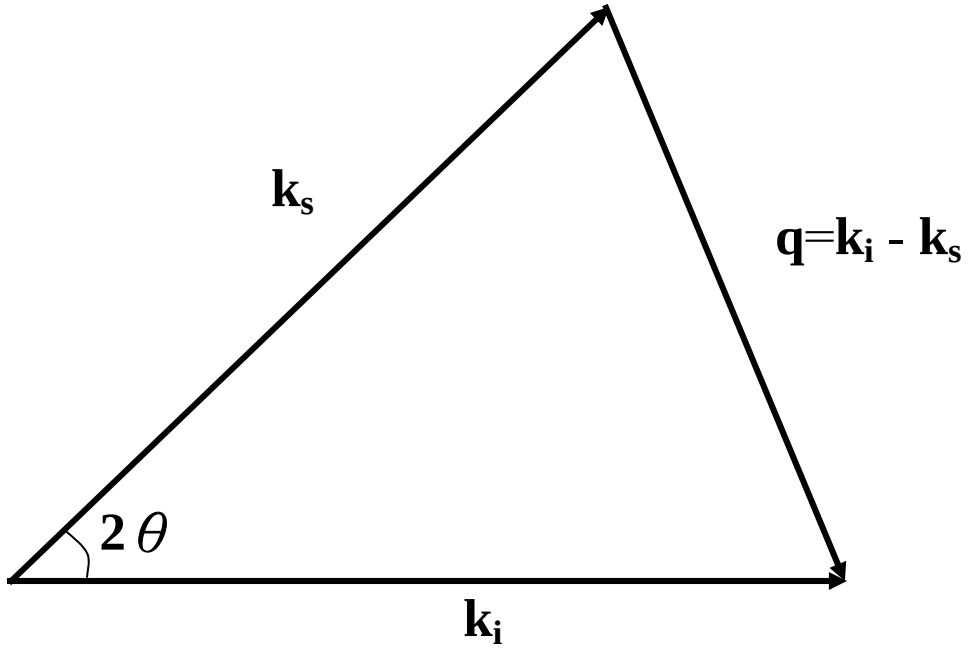

$$k_i = |\mathbf{k_i}| = \frac{2\pi}{\lambda} \quad \text{and} \quad k_s = |\mathbf{k_s}| = \frac{2\pi}{\lambda}$$

$$q = |\mathbf{q}| = |\mathbf{k_i} - \mathbf{k_s}| = \frac{4\pi}{\lambda}\sin\theta$$

Figure 1-4 Relationship between wave vectors and momentum transfer for elastic scattering.

Neutrons have high penetration (low absorption) for most elements, making neutron scattering a bulk probe and allowing sample environments to be designed with materials such as quartz, aluminum, etc. Neutrons are sensitive to the neutron scattering length density of the sample which varies randomly with atomic number and are independent of the momentum transfer, q. Neutron scattering intensity for a particulate system can be expressed as [24-26]:

$$I(q) = k_n \phi P(q) S(q) \qquad (1.4)$$

where ϕ is the volume fraction of the scatterers, *P(q)* is the single particle form factor (intraparticle interference), and *S(q)* is the structure factor (interparticle interference), and k_n ($\text{molecule} \times \text{mole} / \text{cm}^4$) is the contrast factor for neutrons and can be expressed as

$$k_n = N_a \left(\frac{b_A}{v_A} - \frac{b_B}{v_B} \right)^2 \qquad (1.5)$$

where N_a is Avogadro's number and b_i is the neutron scattering length for species i in

the mixture. v_i is the specific volume of species *i*. Therefore by using the fact that the neutron scattering lengths of deuterium and hydrogen, 0.6647 and -0.3741×10^{-12} cm, respectively, are significantly different, deuterium labeling can be used to enhance the contrast.

Comparison of various scattering techniques is summarized in Table 1-1. The small-angle neutron and x-ray scattering (SANS and SAXS) methods are useful for polymer research because they probe size from the near atomic to the near micron.

Table 1-1 Comparison of various radiation scattering techniques.

	Neutrons	X-rays	Laser Light
Wavelength	1-15 Å	0.1-5 Å	1μm
Sensitive to	Nuclei Density	Electron Density	Refractive Density
Sample thickness	1-2 mm	< 1mm	1-5mm
Disadvantage	Low flux	Absorption	Dust scattering
Scattering method	SANS, WANS	SAXS, WAXS	SLS

Small-angle scattering techniques have been widely used to determine polymer properties in dilute solution. Information on such relatively large-scale structure is

contained in the intensity of the scattered neutron at small angles, typically at 2θ less than 2^{o}.

1.3 Contrast Match

The neutron scattering length density of a polymer molecule can be greatly enhanced when some or all of the hydrogen in polymer molecules are replaced by deuterium, but the other physical properties of the molecules remain essentially the same. This is so-called deuterium labeling. Considering two different AGP molecules with one of them composed of PS for all generation, and the other one is also composed of PS for all generation except the last generation has been replaced by deuterated PS. The thickness of last generation won't be able to tell from neutron scattering since the scattering length density distribution would be the same for the first AGP molecule, however, since last generation can be distinguished from previous generations by enhanced scattering length density, the thickness can be measured from neutron scattering. The schematic representation is shown in figure 1-5.

The essential purpose of contrast match is to make polymer molecule "invisible" from the neutron scattering by adjusting the composition of

normal/deuterated solvents. For example, considering the AGP molecule composed of polystyrene for all generation except the last generation was composed of deuterated polystyrene. If we dissolve the molecule in the solvent with scattering length density equals the scattering length density of polystyrene, the part of the molecule can be observed from neutron scattering is the last generation. On the other hand, if the molecule is dissolved in the solvent with scattering length density equals deuterated polystyrene, the part of the molecule composed of polystyrene will be observed at this time. The whole molecule will be observed if the molecule is dissolved in the solvent with scattering length density is between that of polystyrene and deuterated polystyrene. The schematic representation is shown in figure 1-6.

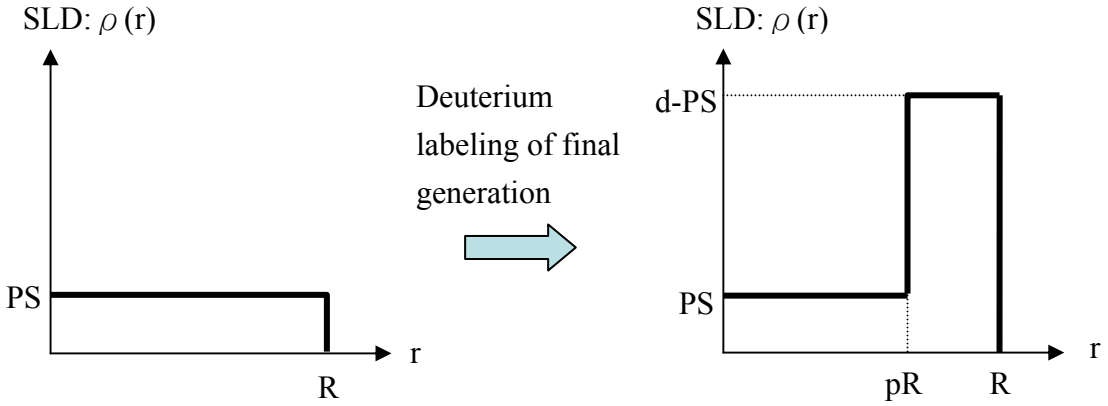

Figure 1-5 schematic representation of the scattering length density distribution of a AGP PS molecule before and after the last generation replaced by deuterated polystyrene. pR is the inner core radius with $0 < p < 1$.

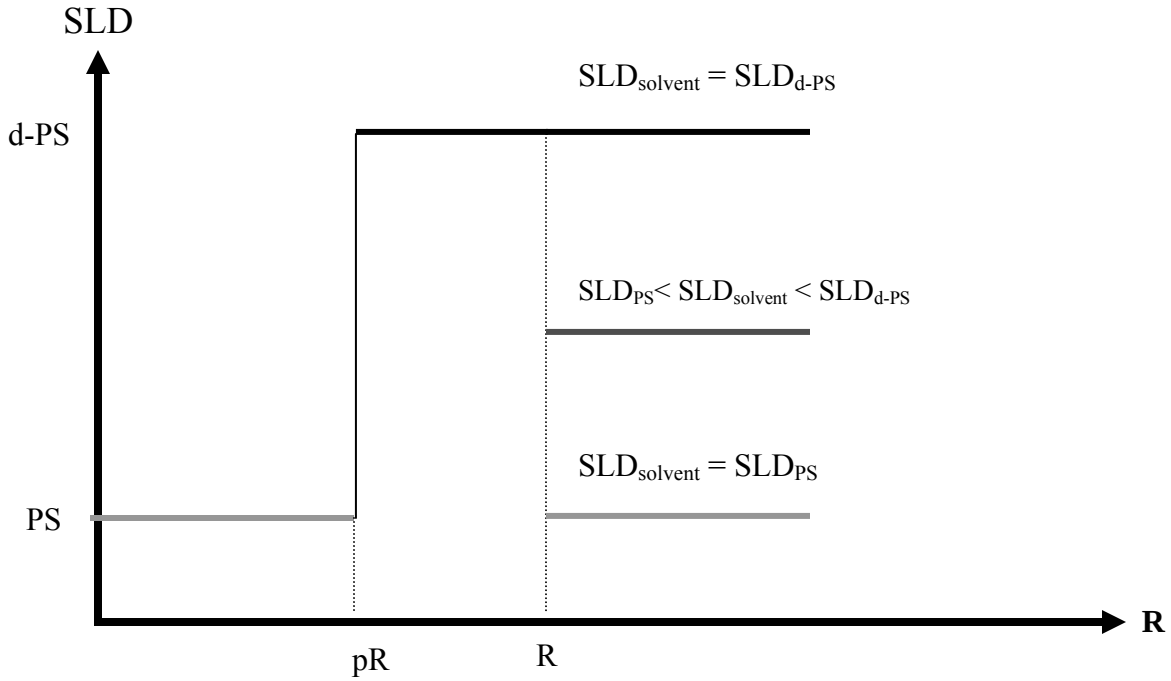

(a)

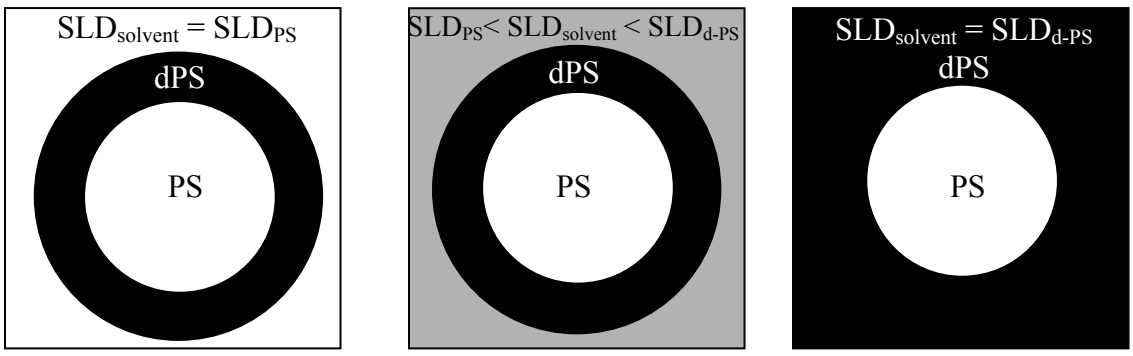

(b)

Figure 1-6 Schemitic representation of contrast match with point of view of (a) scattering length density, (b) a molecule.

Chapter 2

Small Angle Neutron Scattering of Arborescent Graft Polymer Solutions

Arborescent graft polymers are a general class of controlled architecture polymers such as dendrimers and hyperbranched polymers which have been developed in recent years [4-7, 8-17]. These molecules have generated considerable research interest for applications such as coatings, membranes, drug release systems and flow modifiers [10, 19, 20]. For specific applications it is necessary to have detailed information on the intermolecular density profile, molecular size and shape of arborescent graft polymer in solutions. Small angle neutron scattering (SANS) has been used to measure the size and the density profile of arborescent graft polymers in solutions.

2.1 Previous Work

The intramolecular radial density profile in dendrimer molecules has been the topic of a number of both theoretical and computer simulation papers [20, 27-33]. For many of the proposed applications such as monomolecular micelles, flow modifiers

and drug delivery systems, the shape and internal structure of the molecules will play an important role. De Gennes and Hervert was the first group working on this topic. They proposed a model with a minimum density at the center of a dendrimer assuming long flexible spacers between the trifunctional monomer units in an athermal solvent and assumed a fully reacted system [27]. Lescanec and Muthukumar simulated the behavior of dendrimers by a kinetic growth method [28]. Their result showed that dendrimer molecules with flexible branches exhibited a maximum density at the center of the molecule. Mansfield and Klushin used Monte Carlo simulations and also found a maximum in the radial density profile at the center of the molecule with a density gradient to the outside edge of the molecule for smaller dendrimers, which is qualitatively similar to the result of Lescaned and Muthukumar [29]. The larger generation dendrimers (generation 7) exhibited a weak local minimum at the center of the molecule [29]. Murat and Grest have investigated the effect of solvent quality on the density profile and size of dendrimers in solution by molecular dynamics simulations [31]. The density profile of dendrimers under all solvent conditions revealed a high density region near the core, a local minimum, and a constant density plateau followed by a transition zone in which the density decreased gradually [31]. They found that the average mean squared radius of

gyration increased as solvent quality increased. For example the R_g of a generation 8 dendrimer increase by a factor of 1.5 in going from a poor solvent to a good solvent. Stechemesser and Eimer studied the influence of solvent quality on the size of dendrimers in solutions using holographic relaxation spectroscopy and found that the size of the molecules was not significantly different in various quality solvents for low generation dendrimers while solvent quality strongly influenced the size of high generation dendrimers [34]. Recent SANS, however showed that the Rg of a generation 9 dendrimer changed only 10% in this range of solvents [35]. Stechemesser and Eimer suggested that for low generation dendrimers the configuration of the molecules was determined largely by the entropic part of the free energy, while the excluded volume interaction between monomers gave only a minor contribution. According to the work of Naylor et al. the surface and internal volume accessible to the solvent increased with increasing generation number [32, 33]. Thus swelling is expected to increase with increasing solvent quality [34]. Another recent study by Boris and Rubinstein using a self-consistent mean field calculation showed that the density is greatest at the core of the dendrimer and decays monotonically towards the edge of the molecules [20]. Their result is in qualitative agreement with the density profile predicted by Lescanec and Muthukumar. Recently Prosa et al.

studied the internal structure of dendritic polymers using small angle x-ray scattering (SAXS). By comparison of SAXS data with the scattering function calculated for various electron density distributions such as a smooth or rough sphere, they found that the density profile for a generation 10 polyamidoamine (PAMAM) dendrimer does not exhibit any sizable minimum in density near the core [18]. More recent results by Prosa et al. showed that large dendrimers are spherical with a very uniform interior and a very narrow transition zone at the outside [36]. There is a slight polydispersity in sphere radii of less than 10% for generation 10 dendrimers and even dendrimers as small as a generation 4 dendrimer show spherelike characteristics

Sheiko et al. studied the shape of arborescent graft polystyrenes in monomolecular films using scanning atomic force microscopy (AFM) and found that the shape is dependent on the molecular mass and branching density [15]. A highly branched third generation arborescent polymer built from linear chains with a molecular mass of 5000 g/mol had a spherical shape discernible in the dry film, which was indicative of little interpenetration of the molecules. The density and diffusional properties of arborescent polymers were investigated using fluorescence quenching techniques by Frank et al. [16]. They found that the segmental density of arborescent polymers in solution was significantly higher than for linear polystyrene. The

diffusional properties of arborescent polymers indicated an increase in segmental density with increasing generation number.

The physical properties of branched polymers are significantly different from those of linear polymers. For example, the viscosity-molecular mass relation of dendrimers does not obey the Mark-Houwink-Sakurada equation. The intrinsic viscosity varies relatively slowly as a function of molecular mass compared to linear polymers and a maximum is generally observed around generations 3-5 [4, 5]. The viscosity-molecular mass relation of hyperbranched polymers also does obey the Mark-Houwink-Sakurada equation, and the viscosity is anomalously low compared to linear polymers [6]. The variation in the intrinsic viscosity as a function of molecular mass (generation number) for arborescent graft polymer is relatively small, similar to the trend for dendrimers [7]. Gauthier et al. found that the radii of gyration calculated from the intrinsic viscosity measurements for arborescent polymers synthesized from side chains with a molecular mass of 5000 g/mol were essentially identical in a theta solvent (cyclohexane) and a good solvent (toluene). For arborescent polymers with a higher molecular mass side chains (30,000 g/mol), significant expansion was observed in toluene and the increase was largest for the higher generation molecules.

2.2 Synthesis of Arborescent Graft Copolymers

Arborescent graft polymers are branched macromolecules synthesized by successive cycles of functionalization and grafting reactions. The molecules discussed here are synthesized from grafting linear deuterated polystyrene chain onto polystyrene core by Gauthier et al. But the process is not restricted to one type of polymer and has been demonstrated for a polystyrene core and a poly(isoproprene) shell [21]. The synthesis is shown in figure 2-1. Living polymer chains (polymer 1 in figure 2-1) with a narrow molecular weight distribution were obtained by the polymerization of styrene in toluene at room temperature with secbutyllithium. Either isoprene or 2-vinylpyridine was employed as capping agent Z to increase yield of arborescent graft polymer. The arborescent graft polymer back bone, polymer 2, was obtained by adding acetyl chloride to randomly acetylate linear polystyrene chain. The final arborescent graft polymer was achieved by coupling living polystyryl anions with the acetylated polystyrene substrates. By repetition of the acetylization and anionic grafting reactions, higher generation polymers are synthesized. During the grafting reaction, LiCl was added as polystyryllithium reactivity attenuator, which can help to avoid unfavorable side reactions.

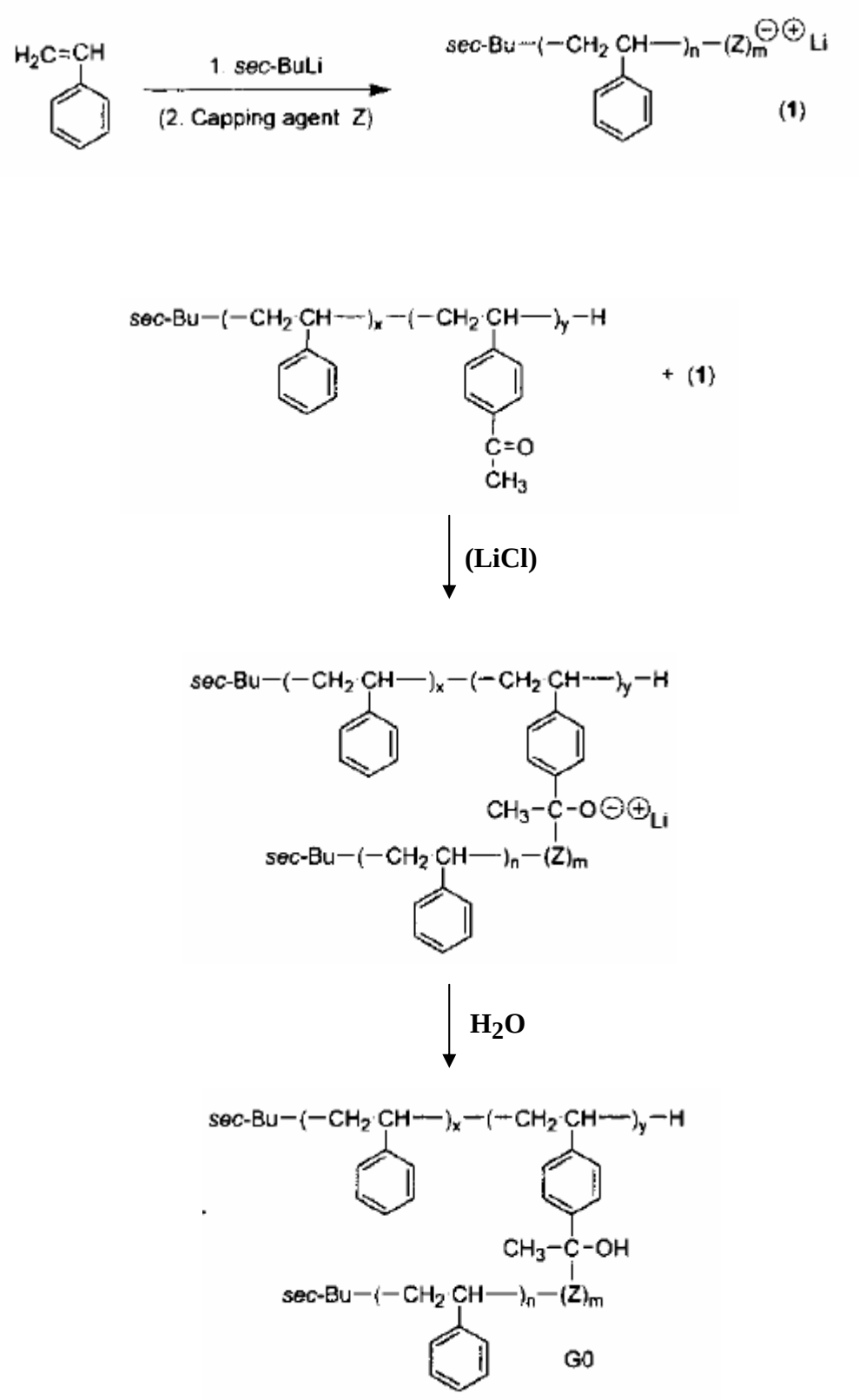

Figure 2-1 Schematic representation of synthesis of arborescent graft polymer [21].

2.3 Experimental

2.3.1 Sample Preparation

The arborescent graft copolymer used in this study were synthesized by Gauthier et al.. The molecular weight mass of the grafted polymer chain for each generation was determined by gel permeation chromatography. The weight average molecular weight of arborescent graft polymers and previous generation core molecule were measured using SANS and light scattering. The characteristics of arborescent graft polymers are given in table 2-1. These polymers have deuterated polystyrene side chains with a molecular mass of 5000g/mol grafted onto the previous generation arborescent graft polymer cores composed of normal polystyrene. The deuterium/hydrogen ratio of a molecule is calculated by eq. (2.1)

$$\mathrm{D/H} = \frac{\left(\mathrm{M}_{\mathrm{w}}^{\mathrm{AGP}}(\mathrm{G}) - \mathrm{M}_{\mathrm{w}}^{\mathrm{PS}}(G-1)\right)\Big/ 112.22}{M_{w}^{PS}(G-1)\Big/ 104.15} \qquad (2.1)$$

where $\mathrm{M}_{\mathrm{w}}^{\mathrm{AGP}}(\mathrm{G})$ and $\mathrm{M}_{\mathrm{w}}^{\mathrm{PS}}(\mathrm{G}\text{-}1)$ are the molar masses of generation G deuterium/hydrogen polystyrene arborescent graft polymer, and the previous generation arborescent graft polymer core composed of normal polystyrene,

Table 2-1 Characteristics of Arborescent Graft Polymers with 5000 $g \times mol^{-1}$ Branches.

Generation	Core	Branches		Graft Copolymer	
	M_W g.mol^{-1}	M_W g.mol^{-1}	M_W/M_n	M_W/g.mol^{-1}	D/H ratio
3	$5.9 \pm 1.5 \times 10^6$	4500	1.07	22×10^6	2.75 ± 1
4	$22.7 \pm 2.2 \times 10^6$	4600	1.09	80×10^6	2.4 ± 0.4

respectively.

Deuterated cyclohexane, deuterated tetrahydrofuran and deuterated toluene were purchased from Cambridge Isotope Laboratories, Inc. Separate polymer solutions were prepared using normal/deuterated cyclohexane, normal/deuterated tetrahydrofuran and normal/deuterated toluene mixture respectively. Each solution was prepared by adjusting the scattering length density of the H/D solvent mixture to equal the scattering length density of polystyrene, deuterated polystyrene, or half of the sum of polystyrene and deuterated polystyrene, and will be specified as core match, shell match, and non match respectively. The polymer concentration of the solution was 1%, and the temperature was kept constant at 25℃.

2.3.2 SANS Measurement

Small angle neutron scattering experiments were carried out at the Center for Neutron Research of the National Institute of Standards and Technology on the 30 meter NIST-NG7 instrument [37, 38]. The data were corrected for empty cell scattering, detectors, sensitivity, sample thickness and transmission and placed on an absolute scale using a calibrated secondary standard and circularly averaged to produce I(q) versus q plots where I(q) is the scattered intensity (cm^{-1}) and q is the scattering vector ($Å^{-1}$).

$$q = \frac{4\pi}{\lambda} Sin\theta \qquad (2.2)$$

The SANS optics are shown in Appendix I.a, I.b, I.c.

2.4 Result and Discussion

2.4.1 Dilute Solution

The single particle properties of individual molecules were studied at dilute polymer concentration in solutions.

2.4.2 Density Profile

2.4.2.1. Small-Angle Neutron Scattering Data

A typical set of SANS data for a generation 3 and 4 arborescent graft polymers in H/D cyclohexane, H/D tetrahydrofuran and H/D toluene are shown in figures 2-2 to 2-4, respectively. The SANS data for both generation arborescent graft polymers dissolved in core-match and non-match solvents clearly show a second interference peak at higher q due to oscillations in the single particle form factor. The scattering data does not show the maxima when the polymer is dissolved in a shell-match solvent.

2.4.2.2 Single Particle Form Factor of Theoretical Scattering Model

For an isotropic system, the scattering intensity does not depend on the orientation and the scattering function for a sphere can be calculated using eq. (2.3)

$$I(q) = \left[\int_0^\infty \rho(r) 4\pi r^2 \frac{\sin qr}{qr} dr \right]^2 \qquad (2.3)$$

where $\rho(r)$ is the density profile of the object. For a hard sphere with a uniform density, the form factor is given by:

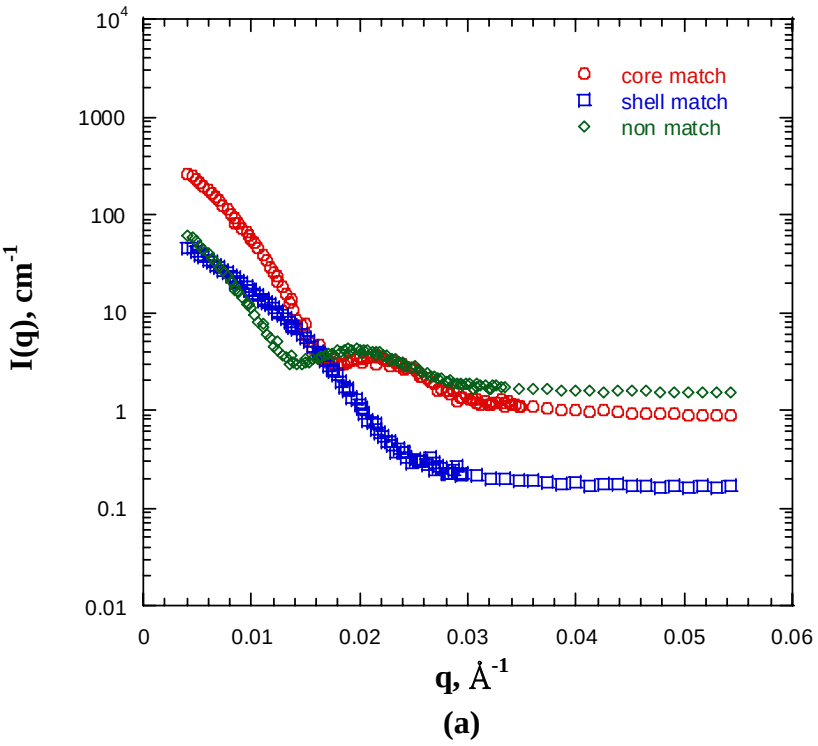

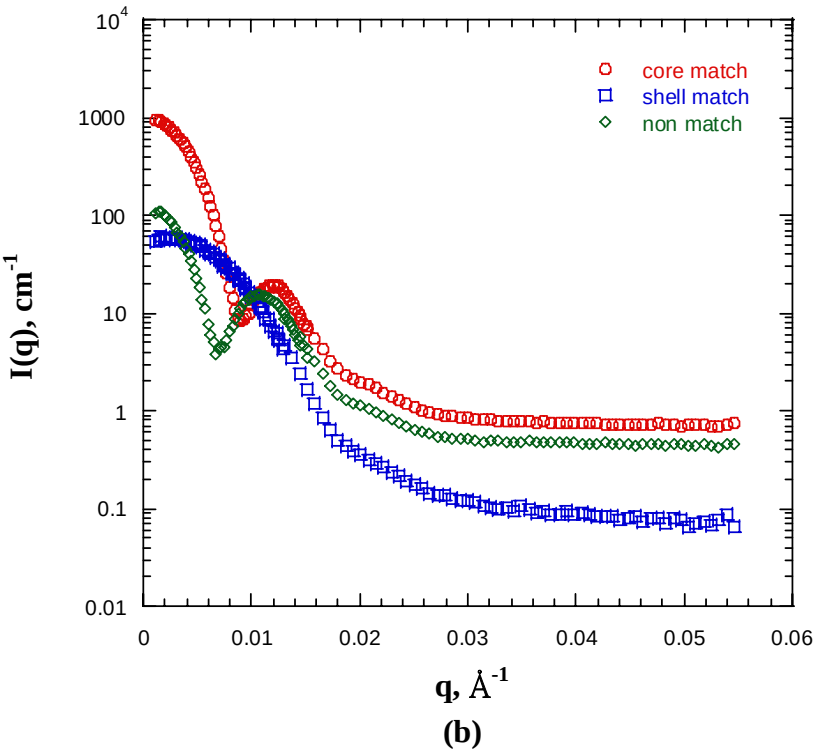

Figure 2-2 SANS curves of (a) generation 3, (b) generation 4 arborescent graft polymers in H/D cyclohexane for H/D ratios.

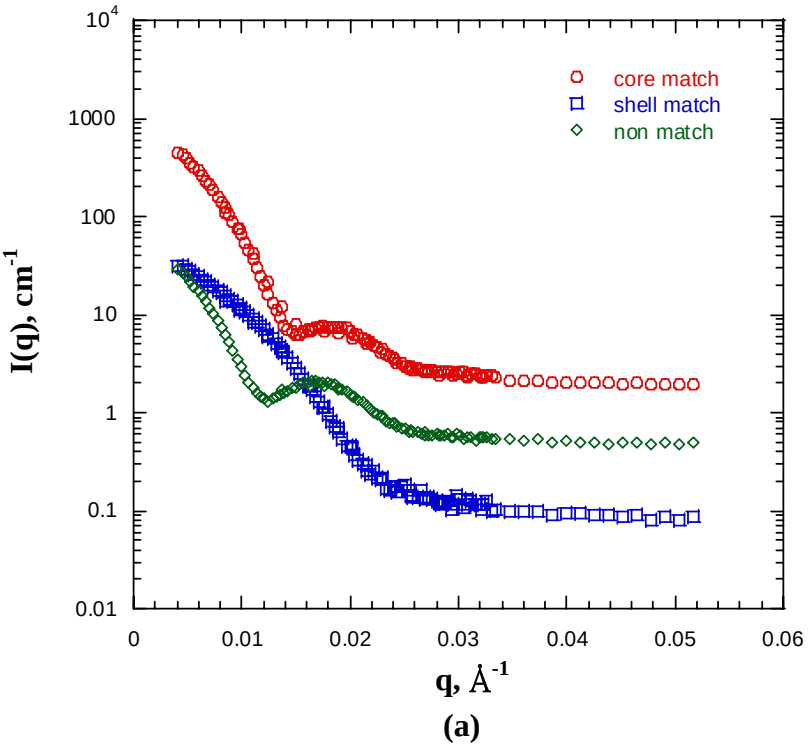

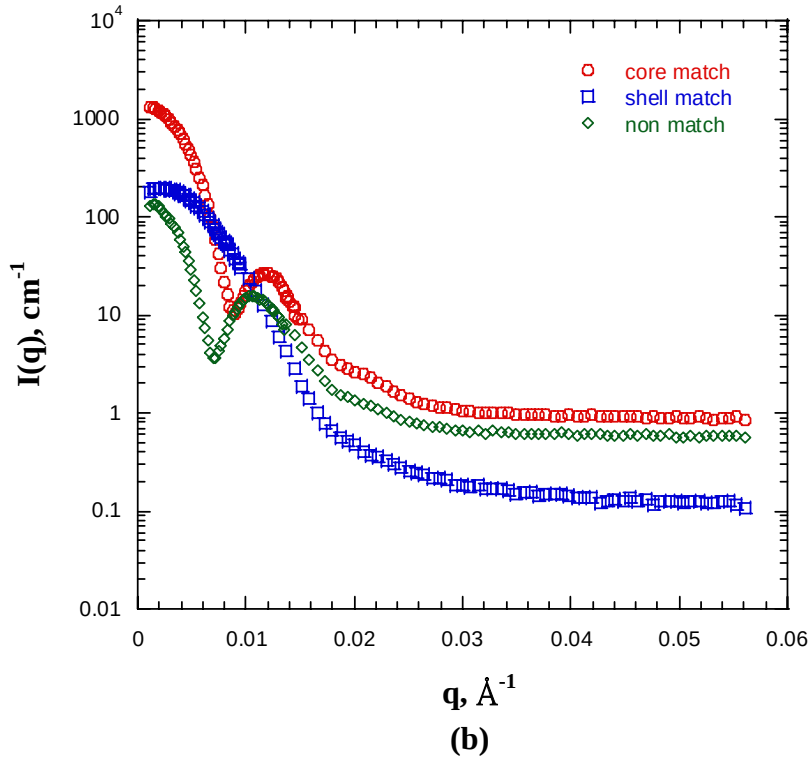

Figure 2-3 SANS curves of (a) generation 3, (b) generation 4 arborescent graft polymers in H/D tetrahydrofuran for H/D ratios.

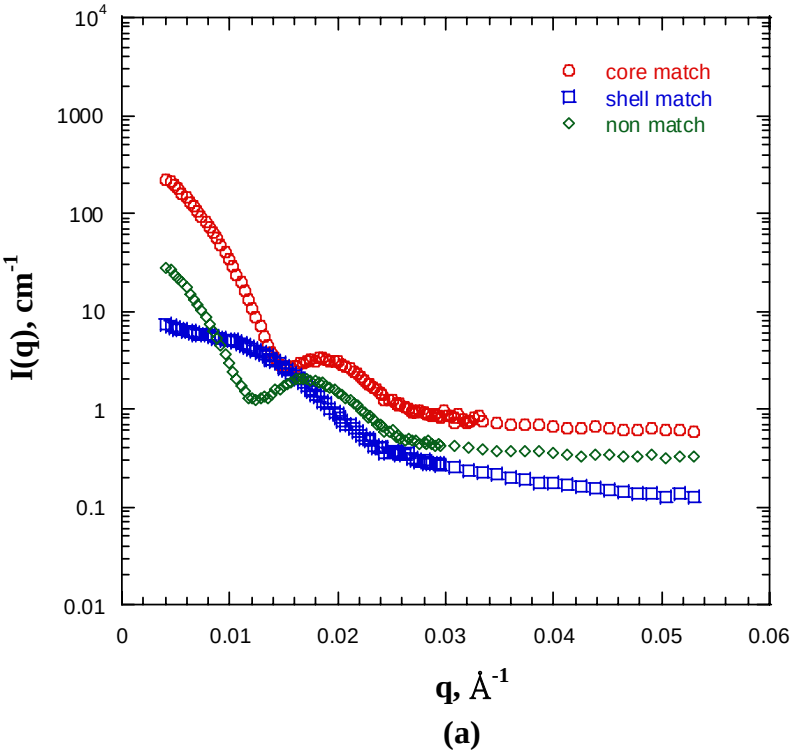

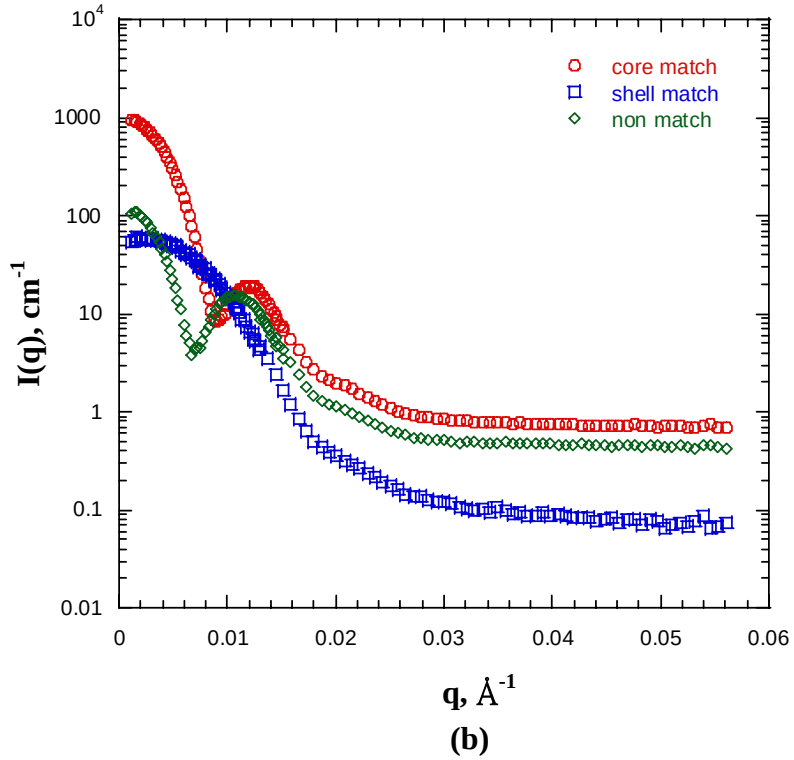

Figure 2-4 SANS curves of (a) generation 3, (b) generation 4 arborescent graft polymers in H/D toluene for H/D ratios.

$$F_0(q) = \frac{3[\sin(qR) - qr\cos(qR)]}{(qR)^3} \qquad (2.4)$$

where R is the hydrodynamic radius of the sphere. The hydrodynamic radius is related to the radius of gyration by $R_g^2 = 3R^2/5$. Eq. (2.4) is also known as Rayleigh geometrical form factor for a uniform sphere of radius R [40].

2.4.2.3 Core-shell Model

Considering spherical particles with a centrosymmetric distribution of scattering length density modeled by a set of M concentric spherical shells, where the j-th shell lies between radii R_{j-1} and R_j and has uniform length density ρ_j. The single particle form factor is given by [41]

$$F_s(q) = V_1(\rho_{1-}\rho_2)F_0(qR_1) + V_2(\rho_{2-}\rho_3)F_0(qR_2) + ...$$
$$.... + V_M(\rho_M - \rho_S)F_0(qR_M) \qquad (2.5)$$

where $F_s(q)$ is the defined form factor, $V_j = {4\pi R_j^3}/{3}$ and $F_0(qR_j)$ is the Rayleigh geometrical form factor for a uniform sphere of radius R as given in eq. (2.4).

When M equals to 2, the structure becomes a simple core-shell model. In our case, the polystyrene forms the core region and the deuterated polystyrene grafted onto it and forms the shell. Taking the total particle radius as R and the inner-core

radius as pR ($0 \le p < 1$), the form factor can be interpreted in a simpler form:

$$F(q) = p^3 C_1 F_0(qpR) + C_2 F_0(qR) \qquad (2.6)$$

where $C_1 = (\rho_1 - \rho_2)V$ and $C_2 = (\rho_2 - \rho_S)V$ with the total volume of the particle being V [41].

Taking polydispersity into consideration, the scattering intensity is averaged over the particle size distribution and becomes:

$$\overline{F_S^2(q)} = \int_0^\infty f(r) F_S^2(qr) dr \qquad (2.7)$$

where f(r) is the normalized probability of finding a particle with a total radius between r and r+dr. The Schulz distribution, which has a wide range of physical applicability, is used as the distribution function. The normalized continuous Schultz distribution is most conveniently written as:

$$f(r) = (z+1)^{z+1} x^z \exp[-(z+1)x] / \bar{r}\Gamma(z+1) \qquad (2.8)$$

where $\bar{r}$ is the mean particle size, $x = r/\bar{r}$, $z = (1-s^2)/s^2$ and $s = \sigma/\bar{r}$, σ^2 is the variance of the distribution. The size-averaged scattering function for a Schultz-distribution core-shell sphere can be obtained from eqs. (2.6), (2.7) and (2.8):

$$\overline{\langle F(q)\rangle_q} = p^3 C_1 t_1(qp\bar{r}) + C_2 t_1(q\bar{r}) \qquad (2.9)$$

$$\overline{\langle F^2(q)\rangle_q} = p^6 C_1^2 t_2(qp\bar{r}) + C_2^2 t_2(q\bar{r}) + 2C_1 C_2 t_3(q\bar{r}, p) \qquad (2.10)$$

where the functions t_i are defined as

$$t_1(y) = \left(\frac{3}{y^3}\right)\left[\frac{\sin z_1 v}{(1+u^2)^{z_1/2}} - \frac{y\cos z_2 v}{(1+u^2)^{z_2/2}}\right], \qquad (2.11)$$

$$t_2(y) = \left(\frac{9}{2z_1 y^6}\right)\left\{z_1\left[1 - \frac{\cos z_1 w}{(1+4u^2)^{z_1/2}} - \frac{2y\sin z_2 w}{(1+4u^2)^{z_2/2}}\right] + y^2 z_2\left[1 + \frac{\cos z_3 w}{(1+4u^2)^{z_3/2}}\right]\right\} \qquad (2.12)$$

$$t_3(y,p) = \left(\frac{9}{2z_1 y^6}\right)\left\{z_1\left[\frac{\cos z_1 v_-}{(1+u_-^2)^{z_1/2}} - \frac{\cos z_1 v_+}{(1+u_+^2)^{z_1/2}}\right] + y^2 p z_2\left[\frac{\cos z_3 v_-}{(1+u_-^2)^{z_3/2}} + \frac{\cos z_3 v_+}{(1+u_+^2)^{z_3/2}}\right]\right.$$
$$\left. + z_1\left[\frac{y_- \sin z_2 v_-}{(1+u_-^2)^{z_2/2}} - \frac{y_+ \sin z_2 v_+}{(1+u_+^2)^{z_2/2}}\right]\right\} \qquad (2.13)$$

with $y_\pm = (1\pm p)y$, $u_\pm = y_\pm / z_1$ and $v_\pm = arctgu_\pm$. Eq. (2.10) will be used to fit the experiment data and provide the information for hydrodynamic radius, scattering

length density of core and shell, and polydispersity.

The core-shell model with polydispersity based on eq. (2.10) was used to fit the scattering data based on procedure written for IGOR software (Wavemetrics, Inc.). The procedures were written by Dr. Steve Kline at the Center for Neutron Research of the National Institute of Standards and Technology [42]. The variables are the "scale" which is the volume fraction of swollen arborescent graft polymers, core radius, shell thickness, polydispersity, scattering length density of core, scattering length density of shell, scattering length density of the solvent. Figures 2-5 to 2-13 show the experimental scattering data, the calculated scattering from core-shell model with and without polydispersity. Fitting results are shown in tables 2-2 to table 2-7.

From the result of the fitting, the size of a molecule in core-match solvents is almost the same size as that of a molecule in the non-match solvents and is in general larger than that of a molecule in the shell-match solvents. From the contrast match point of view, when the scattering length density is adjusted to be the same as deuterated polystyrene, ideally, the only part observed in the scattering experiment would be the polystyrene molecule core, and a similar but reverted situation is for the core-match experiment. However, the molecule observed in the core-match solvents should be treated as a hollow sphere and has the same size as the whole molecule

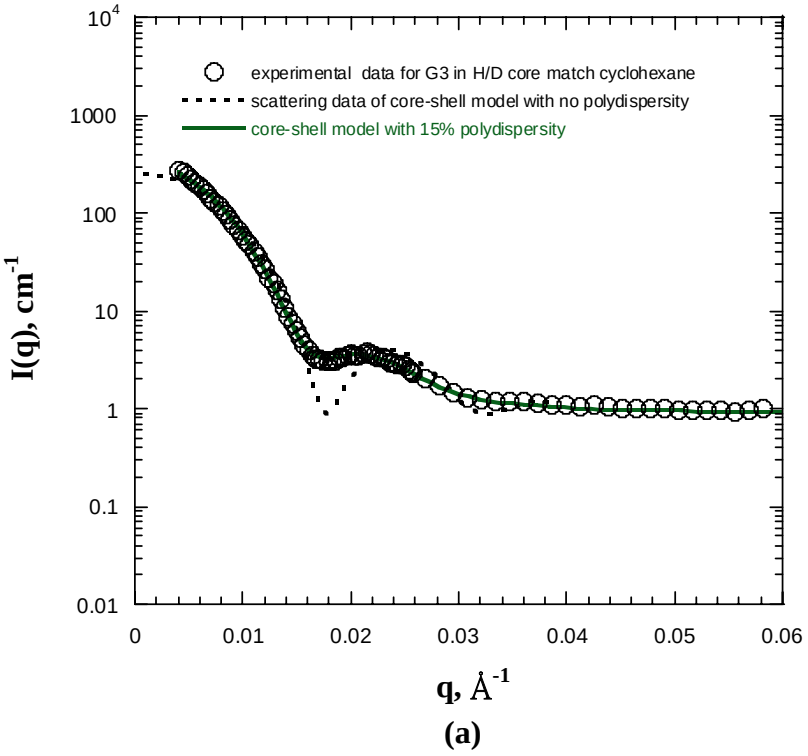

Figure 2-5 Scattering functions for core-shell model law with polydispersity fit to the scattering data for (a) generation 3, (b) generation 4 AGP in H/D core-match cyclohexane.

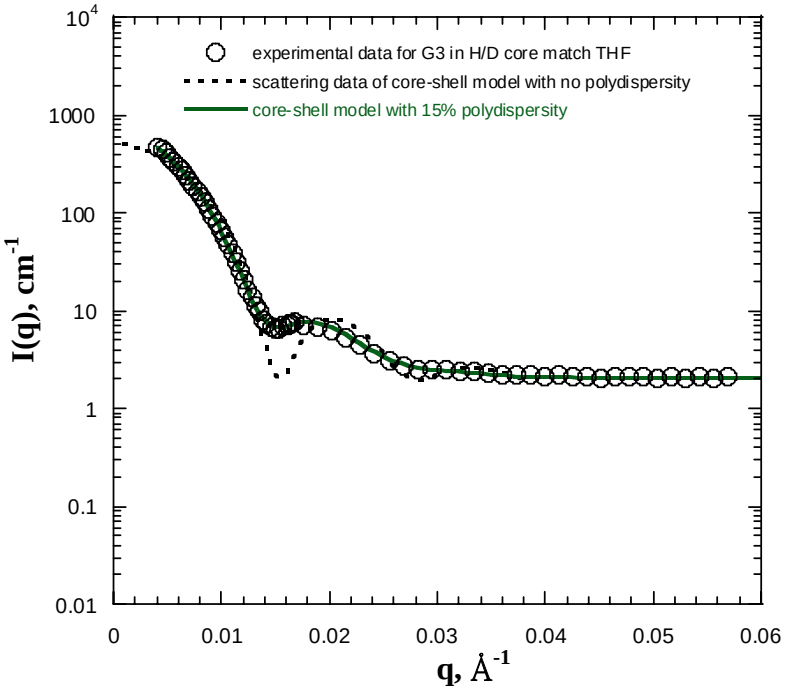

(a)

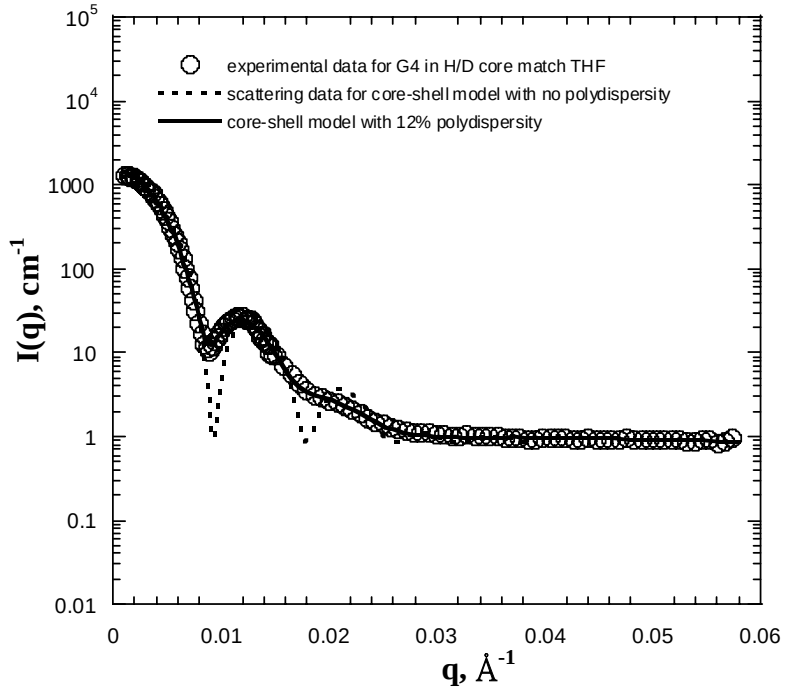

(b)

Figure 2-6 Scattering functions for core-shell model law with polydispersity fit to the scattering data for (a) generation 3, (b) generation 4 AGP in H/D core-match tetrahydrofuran.

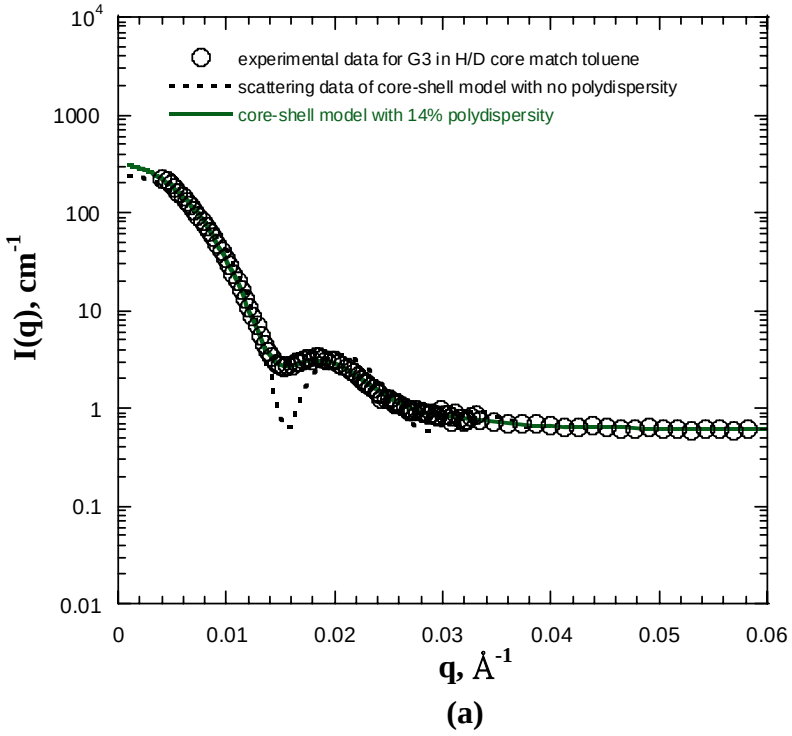

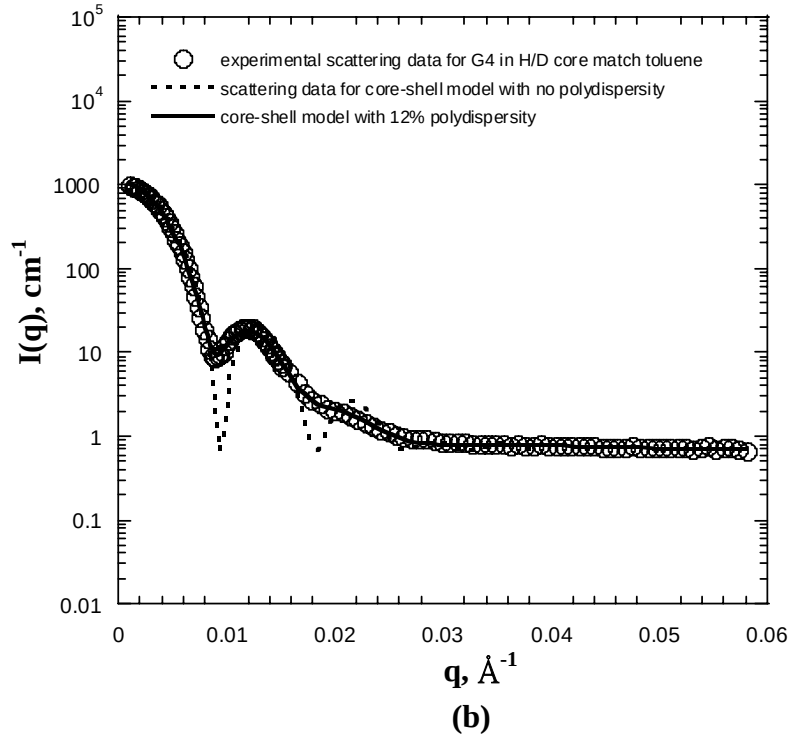

Figure 2-7 Scattering functions for core-shell model law with polydispersity fit to the scattering data for (a) generation 3, (b) generation 4 AGP in H/D core-match toluene.

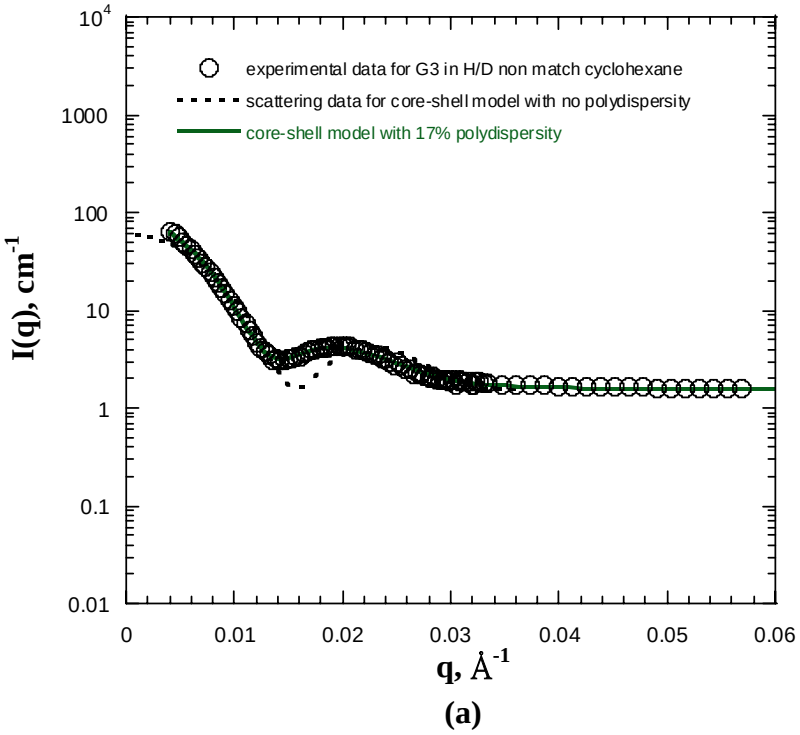

Figure 2-8 Scattering functions for core-shell model law with polydispersity fit to the scattering data for (a) generation 3, (b) generation 4 AGP in H/D non-match cyclohexane.

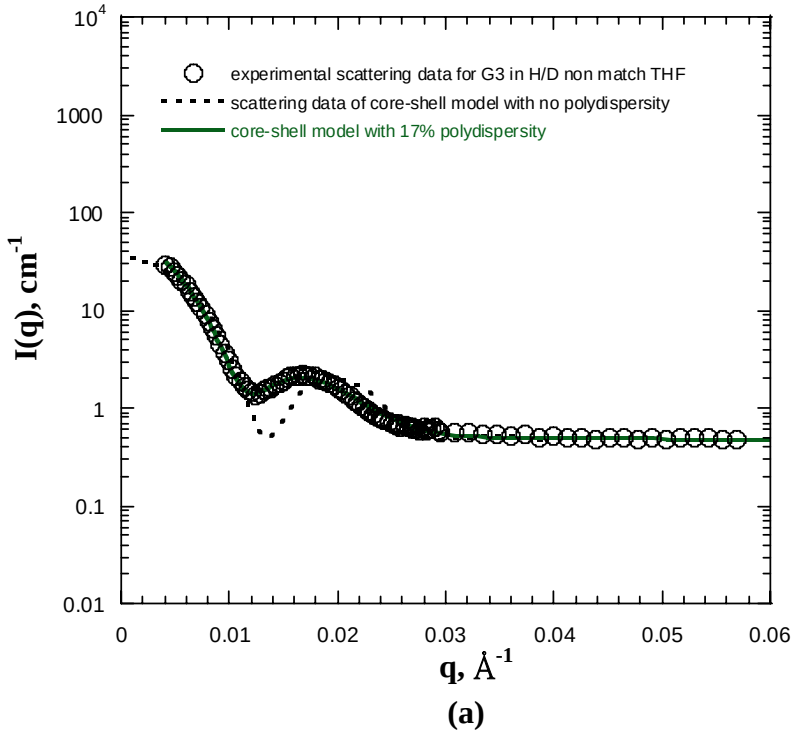

Figure 2-9 Scattering functions for core-shell model law with polydispersity fit to the scattering data for (a) generation 3, (b) generation 4 AGP in H/D non-match tetrahydrofuran.

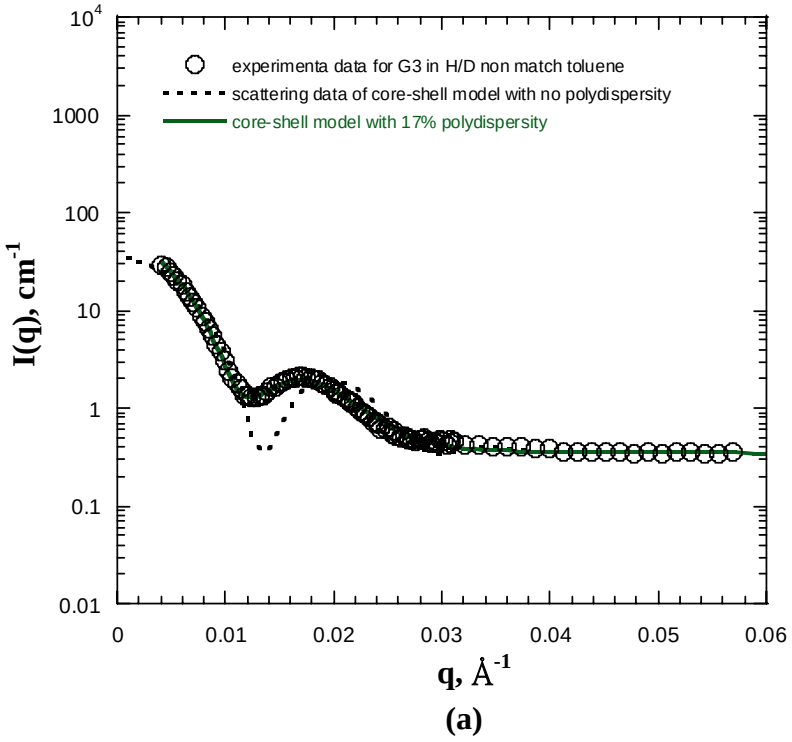

Figure 2-10 Scattering functions for core-shell model law with polydispersity fit to the scattering data for (a) generation 3, (b) generation 4 AGP in H/D non-match toluene.

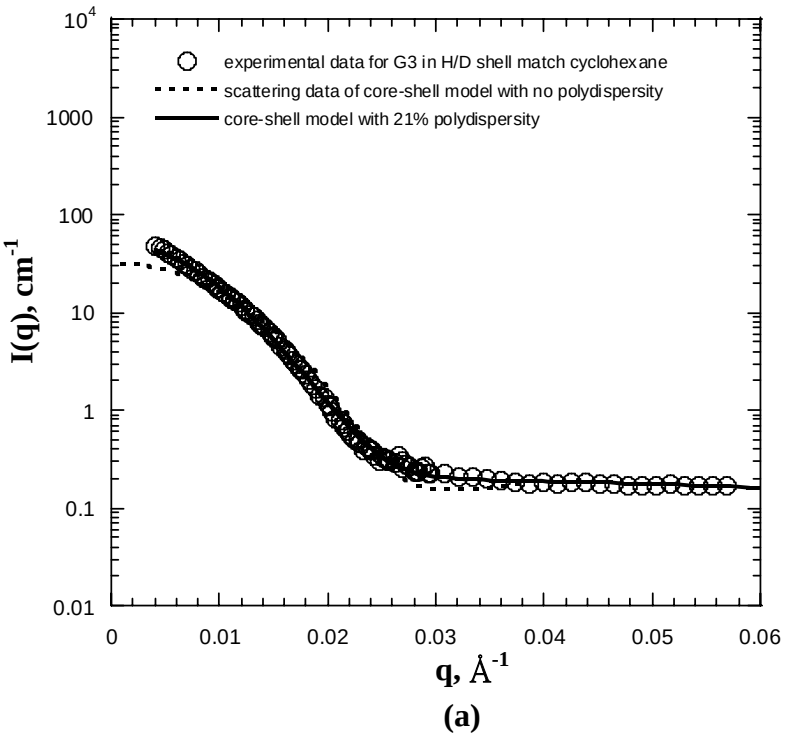

Figure 2-11 Scattering functions for core-shell model law with polydispersity fit to the scattering data for (a) generation 3, (b) generation 4 AGP in H/D shell-match cyclohexane.

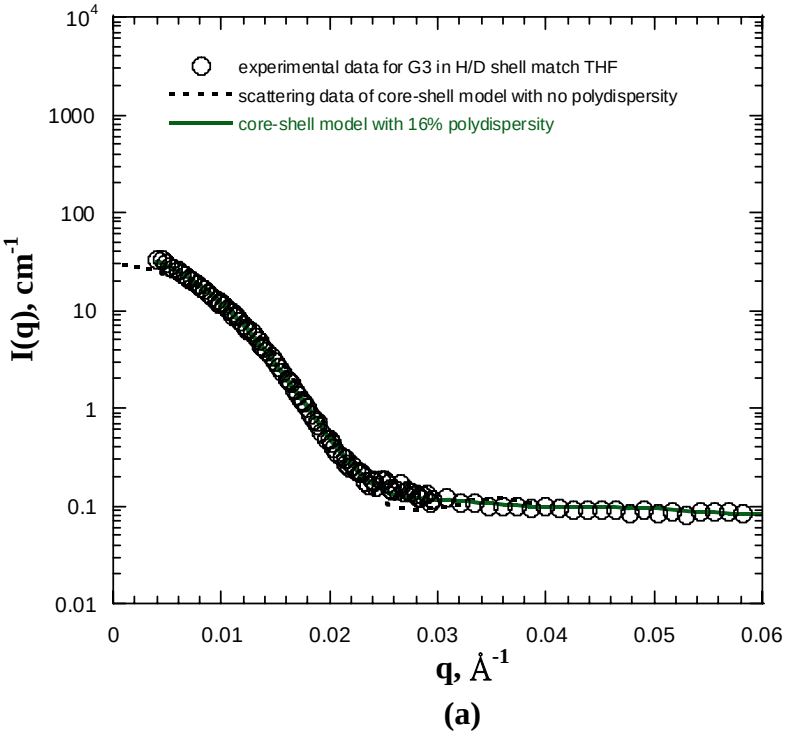

Figure 2-12 Scattering functions for core-shell model law with polydispersity fit to the scattering data for (a) generation 3, (b) generation 4 AGP in H/D shell-match tetrahydrofuran.

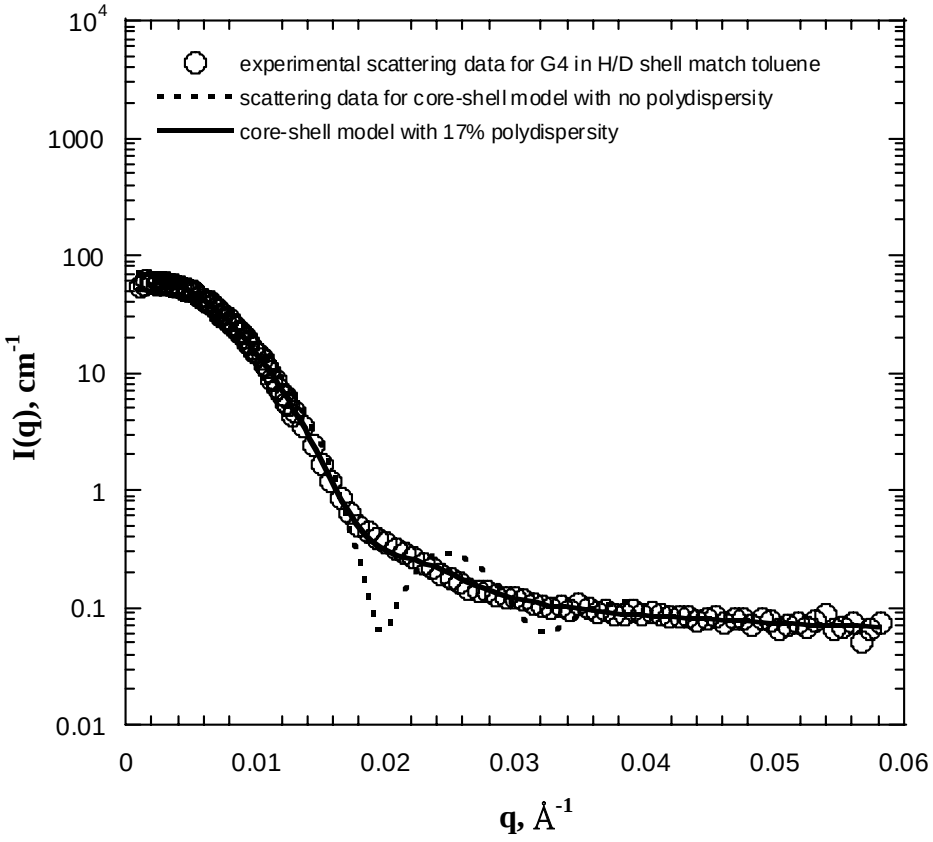

Figure 2-13 Scattering functions for core-shell model law with polydispersity fit to the scattering data for generation 4 AGP in H/D shell-match toluene.

Table 2-2 Fitting result of AGP Generation 4 in H/D Cyclohexane.

	Scale	Core radius (Å)	Shell thickness (Å)	Polydispersity
Core match	0.0141	202	176	0.12
Shell match	0.0045	119	129	0.22
Non match	0.0154	202	176	0.14
	SLD_{core} (molecule/Å^2)	SLD_{shell} (molecule/Å^2)	$SLD_{solvent}$ (molecule/Å^2)	Bkg (cm^{-1})
Core match	1.96×10^{-6}	3.37×10^{-6}	1.40×10^{-6}	1.02
Shell match	3.30×10^{-6}	4.52×10^{-6}	6.30×10^{-6}	0.17
Non match	2.80×10^{-6}	4.68×10^{-6}	3.85×10^{-6}	0.79

Table 2-3 Fitting result of AGP Generation 4 in H/D Tetrahydrofuran.

	Scale	Core radius (Å)	Shell thickness (Å)	Polydispersity
Core match	0.0236	233	203	0.12
Shell match	0.011	224	107	0.19
Non match	0.0231	230	203	0.14
	SLD_{core} (molecule/Å^2)	SLD_{shell} (molecule/Å^2)	$SLD_{solvent}$ (molecule/Å^2)	Bkg (cm^{-1})
Core match	1.72×10^{-6}	2.81×10^{-6}	1.40×10^{-6}	0.86
Shell match	4.02×10^{-6}	5.91×10^{-6}	6.30×10^{-6}	0.10
Non match	3.06×10^{-6}	4.48×10^{-6}	3.85×10^{-6}	0.59

All radii are ± 5Å. SLD_{core} and SLD_{shell} are ± 10%, and background are ± 10%

Table 2-4 Fitting result of AGP Generation 4 in H/D Toluene.

	Scale	Core radius (Å)	Shell thickness (Å)	Polydispersity
Core match	0.022	228	202	0.13
Shell match	0.0041	129	108	0.17
Non match	0.023	228	202	0.15
	SLD_{core} (molecule/Å^2)	SLD_{shell} (molecule/Å^2)	$SLD_{solvent}$ (molecule/Å^2)	Bkg (cm^{-1})
Core match	1.65×10^{-6}	2.66×10^{-6}	1.40×10^{-6}	0.69
Shell match	3.76×10^{-6}	4.24×10^{-6}	5.68×10^{-6}	0.06
Non match	3.00×10^{-6}	4.45×10^{-6}	3.85×10^{-6}	0.44

Table 2-5 Fitting result of AGP Generation 3 in H/D Cyclohexane.

	Scale	Core radius (Å)	Shell thickness (Å)	Polydispersity
Core match	0.0125	110	132	0.15
Shell match	0.0075	93	104	0.21
Non match	0.013	110	132	0.18
	SLD_{core} (molecule/Å^2)	SLD_{shell} (molecule/Å^2)	$SLD_{solvent}$ (molecule/Å^2)	Bkg (cm^{-1})
Core match	2.50×10^{-6}	3.33×10^{-6}	1.40×10^{-6}	0.90
Shell match	3.17×10^{-6}	5.38×10^{-6}	6.30×10^{-6}	0.15
Non match	2.90×10^{-6}	4.91×10^{-6}	3.85×10^{-6}	1.59

All radii are ± 5Å. SLD_{core} and SLD_{shell} are ± 10%, and background are ± 10%

Table 2-6 Fitting result of AGP Generation 3 in H/D Tetrahydrofuran.

	Scale	Core radius (Å)	Shell thickness (Å)	Polydispersity
Core match	0.0216	130	149	0.15
Shell match	0.0133	111	120	0.16
Non match	0.0225	130	150	0.18
	SLD_{core} (molecule/Å^2)	SLD_{shell} (molecule/Å^2)	$SLD_{solvent}$ (molecule/Å^2)	Bkg (cm^{-1})
Core match	2.31×10^{-6}	3.09×10^{-6}	1.40×10^{-6}	1.98
Shell match	4.39×10^{-6}	5.81×10^{-6}	6.30×10^{-6}	0.07
Non match	3.41×10^{-6}	4.35×10^{-6}	3.85×10^{-6}	0.48

Table 2-7 Fitting result of AGP Generation 3 in H/D Toluene.

	Scale	Core radius (Å)	Shell thickness (Å)	Polydispersity
Core match	0.0202	133	144	0.14
Shell match	x	x	x	X
Non match	0.0213	133	144	0.17
	SLD_{core} (molecule/Å^2)	SLD_{shell} (molecule/Å^2)	$SLD_{solvent}$ (molecule/Å^2)	Bkg (cm^{-1})
Core match	2.15×10^{-6}	2.62×10^{-6}	1.40×10^{-6}	0.59
Shell match	X	X	6.30×10^{-6}	X
Non match	3.42×10^{-6}	4.38×10^{-6}	3.85×10^{-6}	0.34

All radii are ± 5Å. SLD_{core} and SLD_{shell} are ± 10%, and background are ± 10%

while the size of the molecule observed in the shell-match solvents should be smaller. Even though the scattering data for the molecule dissolved in the shell-match solvent can be fit well using the core-shell model, the obtained parameters are difficult to interpret in a physically meaningful way. Attempts were made to fit the data with a hard sphere model (with polydispersity), but the fit did not converge. From the fit results for molecules dissolving in core-match and non-match solvents, the core and shell scattering length densities do not equal to the calculated length scattering densities of pure polystyrene or deuterated polystyrene (1.40×10^{-6} molecule/Å^2 and 6.30×10^{-6} molecule/Å^2, respectively). Since the reacting sites are randomly distributed among the arborescent graft polymer core during the synthesis, it is reasonable for the deuterated polystyrene to penetrate into the core. Thus we can assume that there is a region inside the arborescent graft polymer molecule where polystyrene and deuterated polystyrene are mixing together. When a molecule is dissolved in a solvent, the solvent that penetrates into the molecule may also affect the final result scattering length density. The effect increases with the quality of solvent since the solvent with higher quality introduces more solvent into the molecule. The illustration is shown in figure 2-14. We can attempt to account for this effect with the following equations combined with the results from the fits of the

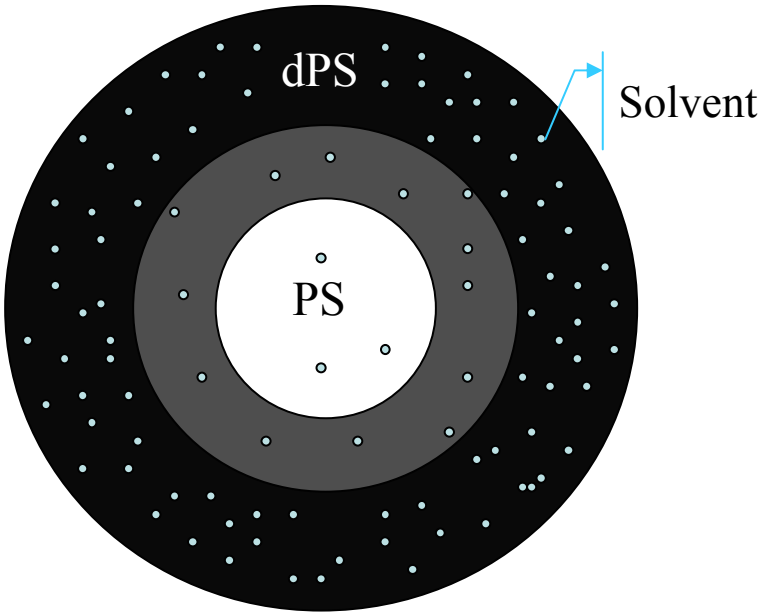

(a)

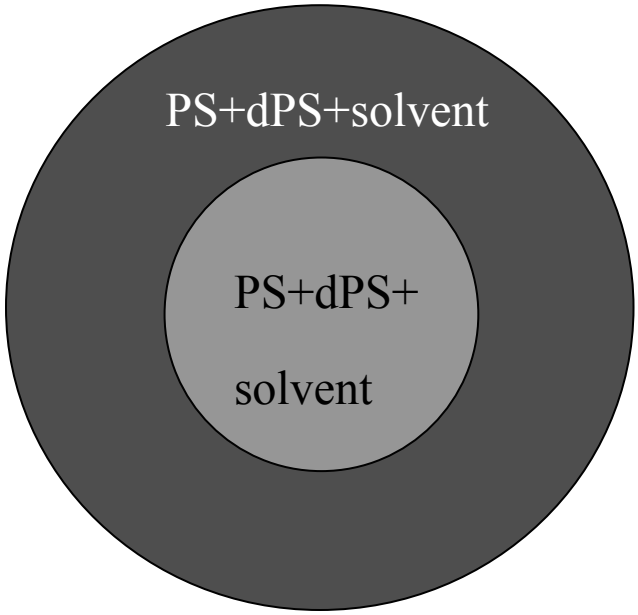

(b)

Figure 2-14 Schematic representation of the structure of a AGP molecule in solvent (a) real situation (b) presented by core-shell model.

scattering data. Consider the core region of the molecule

$$\phi_{\mathrm{PS}}^{\mathrm{core}} \times \mathrm{SLD}_{\mathrm{PS}} + \phi_{\mathrm{dPS}}^{\mathrm{core}} \times \mathrm{SLD}_{\mathrm{dPS}} + \phi_{\mathrm{solvent}}^{\mathrm{core}} \mathrm{SLD}_{\mathrm{sol-corematch}} = \mathrm{SLD}_{\mathrm{core-corematch}} \quad (2.14)$$

$$\phi_{\mathrm{PS}}^{\mathrm{core}} \times \mathrm{SLD}_{\mathrm{PS}} + \phi_{\mathrm{dPS}}^{\mathrm{core}} \times \mathrm{SLD}_{\mathrm{dPS}} + \phi_{\mathrm{solvent}}^{\mathrm{core}} \mathrm{SLD}_{\mathrm{sol-nonmatch}} = \mathrm{SLD}_{\mathrm{core-nonmatch}} \quad (2.15)$$

$$\phi_{\mathrm{PS}}^{\mathrm{core}} + \phi_{\mathrm{dPS}}^{\mathrm{core}} + \phi_{\mathrm{solvent}}^{\mathrm{core}} = 1 \quad (2.16)$$

where $\mathrm{SLD}_{\text{core-core match}}$, $\mathrm{SLD}_{\text{core-nonmatch}}$ are the fitting result of $\mathrm{SLD}_{\mathrm{core}}$ in core-match and non-match solvents, respectively. $\mathrm{SLD}_{\mathrm{PS}} = 1.40\times10^{-6}$ molecule/Å^2, $\mathrm{SLD}_{\mathrm{dPS}} = 6.30\times10^{-6}$ molecule/Å^2, $\mathrm{SLD}_{\text{sol-corematch}} = 1.40\times10^{-6}$ molecule/Å^2, and $\mathrm{SLD}_{\text{sol-nonmatch}} = 3.85\times10^{-6}$ molecule/Å^2. ϕ_{PS}^{core}, ϕ_{dPS}^{core}, and $\phi_{solvent}^{core}$ are the volume fraction of polystyrene, deuterated polystyrene and solvent in the core region of the molecule. From the fitting result, there should be the same amount of polystyrene, deuterated polystyrene and solvent in the core region of molecule for core-match solvent and non-match solvent since both results show the same core radius. Therefore, the difference between $\mathrm{SLD}_{\text{core-core match}}$ and $\mathrm{SLD}_{\text{core-nonmatch}}$ should be the result of the difference between the scattering length densities of the core-match solvent and non-match solvents. Therefore values of ϕ_{PS}^{core}, ϕ_{dPS}^{core}, and $\phi_{solvent}^{core}$ can be obtained by solving eqs. (2.14), (2.15) and (2.16). Density profiles for the shell region of the molecule can be obtained from the same analysis. Density profiles for

generation 3 AGP and generation 4 AGP in different solvents are shown in tables 2-8 to 2-13. Figures 2-15 and 2-16 show the density profiles of molecules dissolved in different solvents compared with what would be expected if the molecule were collapsed as a hard sphere.

From the profiles, it can be concluded that the hydrogenated/deuterated polystyrene mixing zone exists as expected. Nevertheless, we cannot have the exact thickness of the layer and the fractions of each component from the density profiles. The average solvent fraction of the molecule are almost the same for both generation arborescent graft polymers. The polydispersity obtained from the fit of the core-match and non-match solvents are almost equivalent. For these cases we should see essentially the scattering from the whole molecule and it is reasonable that the polydispersity should have the same values. On the other hand, the polydispersity from fitting result when the molecule is dissolved in shell-match solvent represents the size distribution of the total size of the PS core and part of the mixing region and might be expected to be different.

2.4.3 Radius of Gyration

The size of a particle, irrespective of whether it is geometrically defined or

Table 2-8 G4 in cyclohexane.

Core	solvent %	35 ± 3.5 %
	polystyrene %	54 ± 3 %
	d-polystyrene %	11 ± 1 %
Shell	solvent %	49 ± 1 %
	polystyrene %	10 ± 1 %
	d-polystyrene %	41 ± 2 %

Table 2-9 G4 in tetrahydrofuran.

Core	solvent %	54 ± 5 %
	polystyrene %	40 ± 3 %
	d-polystyrene %	6 ± 2 %
Shell	solvent %	67 ± 1 %
	polystyrene %	4 ± 1 %
	d-polystyrene %	29 ± 1 %

Table 2-10 G4 in toluene.

Core	solvent %	55 ± 5 %
	polystyrene %	40 ± 4 %
	d-polystyrene %	5 ± 1 %
Shell	solvent %	65 ± 4 %
	polystyrene %	7 ± 1 %
	d-polystyrene %	28 ± 2 %

Table 2-11 G3 in cyclohexane.

Core	solvent %	31 ± 3 %
	polystyrene %	50 ± 2 %
	d-polystyrene %	19 ± 1 %
Shell	solvent %	43 ± 3 %
	polystyrene %	12 ± 1 %
	d-polystyrene %	45 ± 3 %

Table 2-12 G3 in tetrahydrofuran.

Core	solvent %	53 ± 5 %
	polystyrene %	30 ± 3 %
	d-polystyrene %	17 ± 2 %
Shell	solvent %	63 ± 3 %
	polystyrene %	5 ± 1 %
	d-polystyrene %	32 ± 2 %

Table 2-13 G3 in toluene.

Core	solvent %	54 ± 5 %
	polystyrene %	32 ± 2 %
	d-polystyrene %	14 ± 2 %
Shell	solvent %	62 ± 4 %
	polystyrene %	11 ± 1 %
	d-polystyrene %	27 ± 3 %

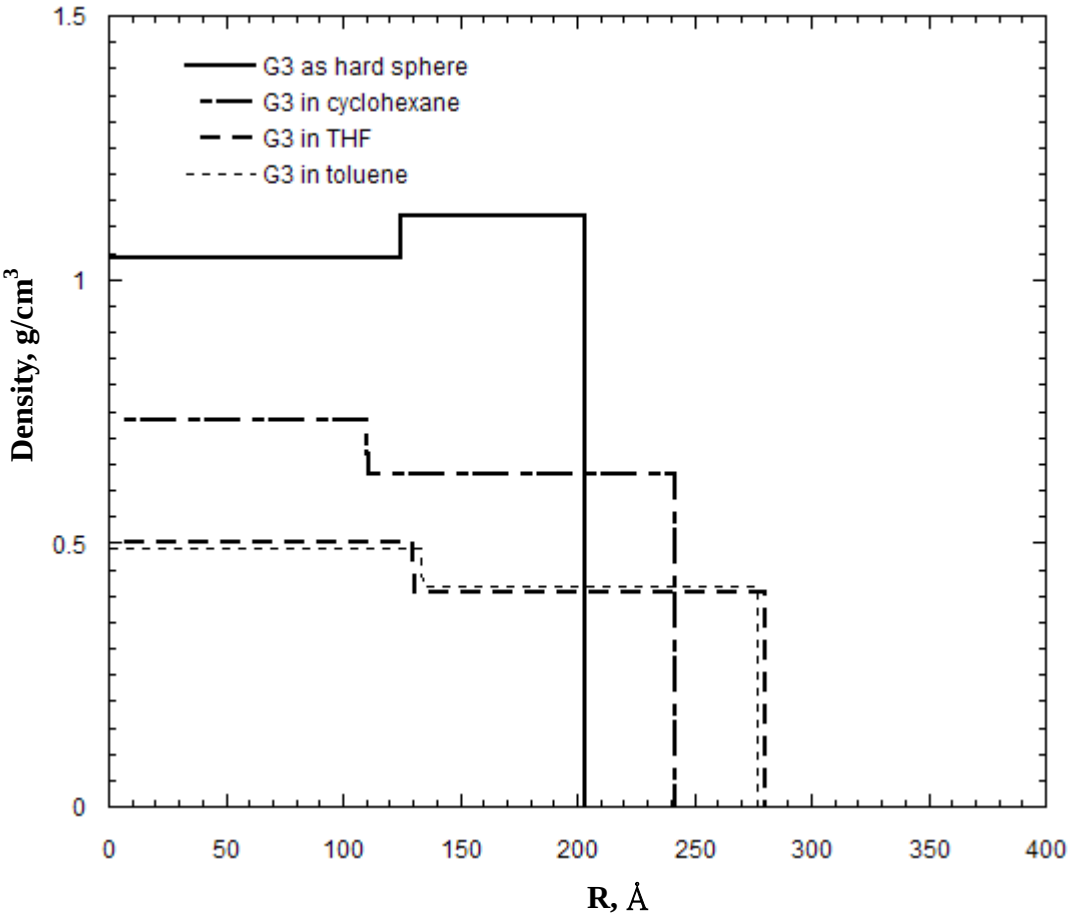

Figure 2-15 Density profiles of generation 3 AGP in different solvents and taken as a hard sphere.

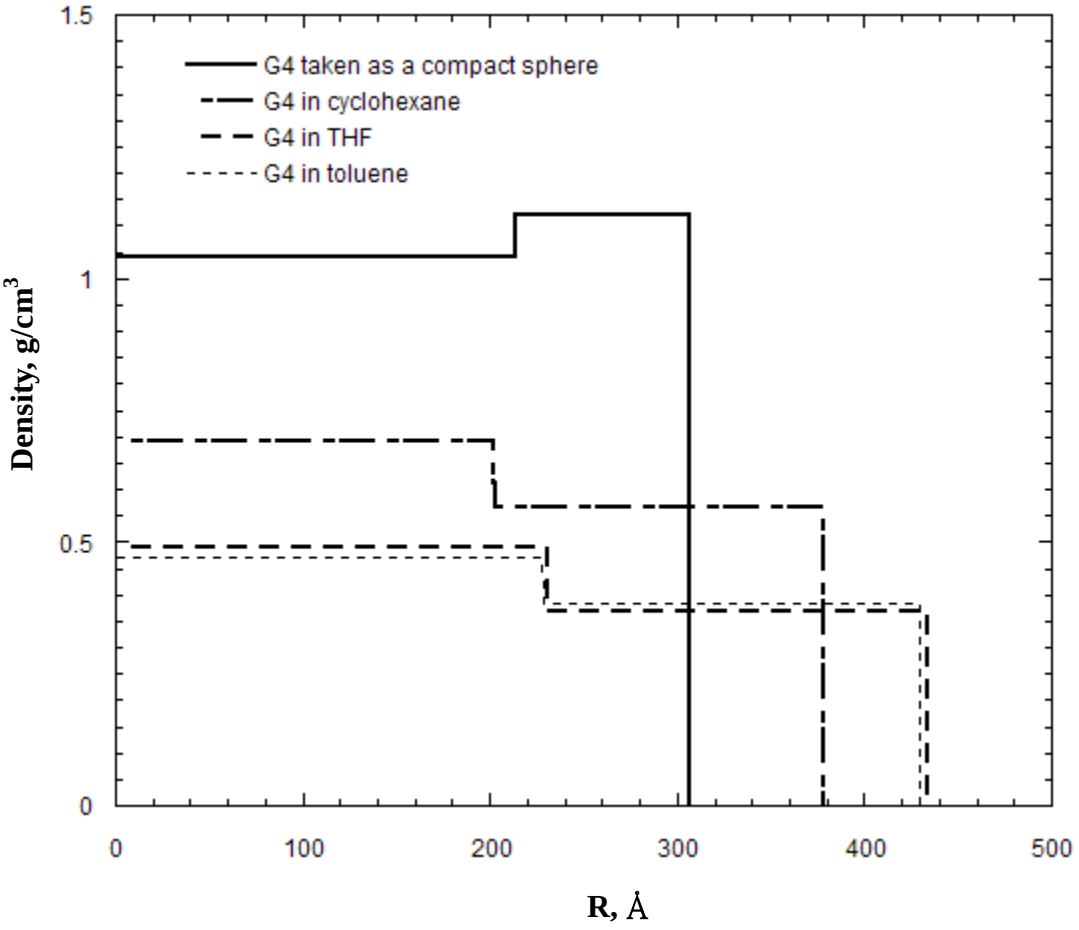

Figure 2-16 Density profiles of generation 4 AGP in different solvents and taken as a hard sphere.

irregular in shape, can be conveniently characterized by its *radius of gyration* which is defined as the mass weighted root-mean-square average of the magnitude of the vectors leading from the center-of-mass to the points making up the rigid body [39]. The radius of gyration was first measured using Guinier plots at small q. For dilute non-interacting particles the scattering intensity is expected to obey Guinier's law:

$$I(q) = I(0)\exp\left(-\frac{R_g^2 q^2}{3}\right) \qquad (2.17)$$

where R_g is radius of gyration of the object. The Guinier plots of lnI(q) versus q^2 for generation 3 arborescent graft copolymer in H/D cyclohexane, H/D tetrahydrofuran, H/Dtoluene are shown for all solvent ratios in figure 2-17. The Guinier plots for generation 4 arborescent graft copolymer in H/D cyclohexane, H/D tetrahydrofuran, H/D toluene are shown for all H/D ratio in figure 2-18. The radius of gyration results of generation 3 and generation 4 arborescent graft polymers are shown in table 2-14 compared with the hydrodynamic radius. The R_g in H/D toluene for the shell-match condition is noticeably smaller than that in the other two shell-match solvents. The scattering length density for deuterated toluene is 5.68×10^{-6} (molecule/Å^2) which is less than scattering length density of deuterated polystyrene. Therefore it is not

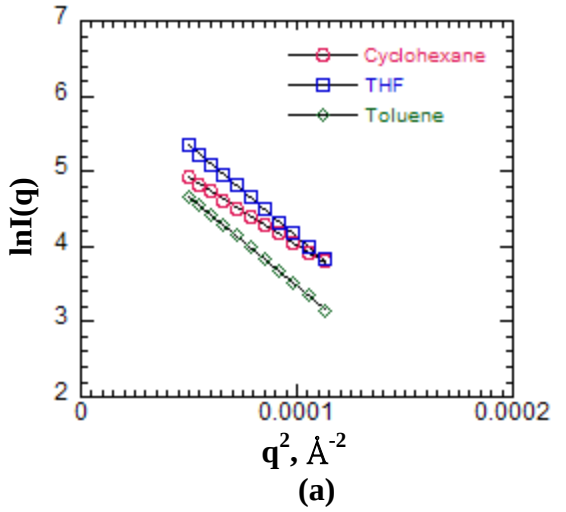

Figure 2-17 Guinier plot at small q for generation 3 (a) core match series, (b) non matches, (c) shell matches.

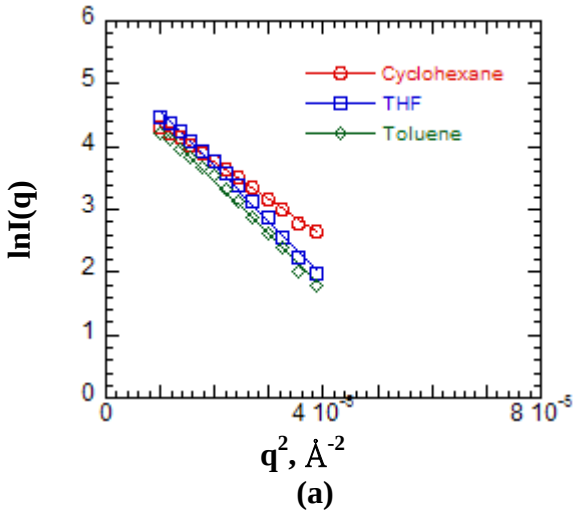

Figure 2-18 Guinier plot at small q for generation 4 (a) core match series, (b) non matches, (c) shell matches.

Table 2-14 Comparison of hydrodynamic radius and the R_g observed from Guinier Region for generation 4 and generation3.

G4			G3		
	R_h	R_g		R_h	R_g
CH-core match	378	358	CH-core match	242	229
THF-core match	436	422	THF-core match	279	267
Toluene-core match	430	417	Toluene-core match	277	266
CH-non match	378	422	CH-non match	242	248
THF-non match	433	513	THF-non match	280	288
Toluene-non match	430	507	Toluene-non match	277	290
CH-shell match	248	241	CH-shell match	197	177
THF-shell match	331	256	THF-shell match	231	184
Toluene-shell match	237	220	Toluene-shell match	x	96

possible to fully match the deuterated polystyrene shell in H/D toluene. Our possible explanation for the smaller R_g when the molecule is dissolved in deuterated toluene is that the degree of contrast matching of the shell maybe higher in deuterated toluene than in the H/D cyclohexane or H/D THF whose scattering length density can be more closely adjusted to deuterated polystyrene. To test this idea, several polymer solutions in H/D cyclohexane with different average solvent scattering length densities were prepared for the SANS measurement. The solvent scattering length densities ranged from 5.9×10^{6} (molecule/Å^2) down to 4.7×10^{6} (molecule/Å^2). The scattering data and Guinier plots are shown in figure 2-19. The scattering intensity decreases with decreasing solvent scattering length density, and the

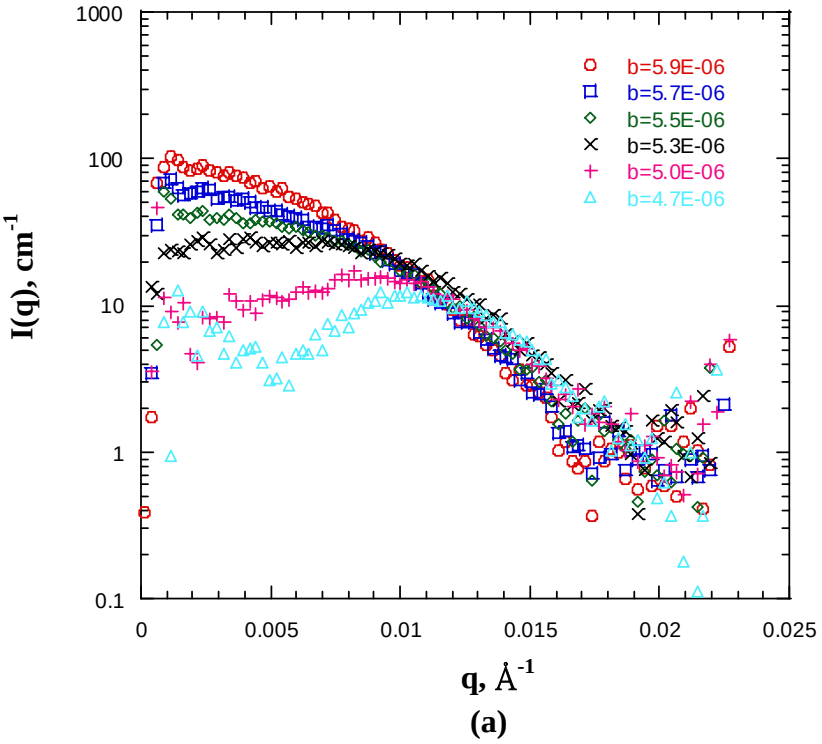

(a)

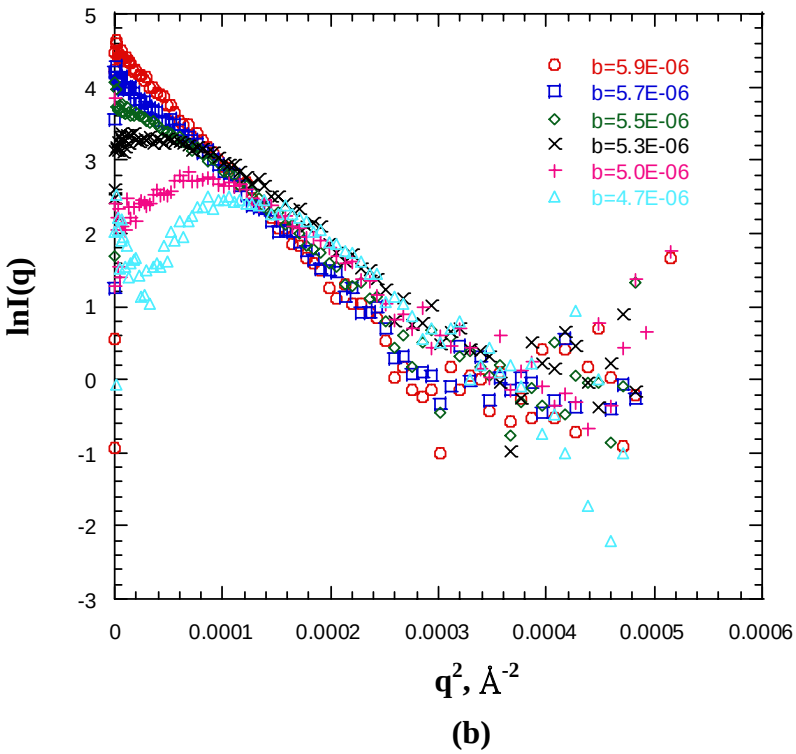

(b)

Figure 2-19 Scattering data (a) and Guinior plot (b) of generation 4 AGP in H/D cyclohexane with different scattering length density.

scattering shape changes from a smooth curve to having a peak at low q which is consistent with the shape as was measured for the non-match solution. In the Guinier plots, the slope increases as the solvent scattering length density decreases with the slope becoming positive when solvent scattering length density equals 5.0×10^{6} (molecule/Å^2), and becomes negative again when solvent scattering length density equals 4.7×10^{6} (molecule/Å^2). In terms of R_g, radius of gyration decreases as the solvent scattering length density decreases, becomes negative when solvent scattering length density equals 5.0×10^{6} (molecule/Å^2), and back to positive value when the solvent scattering length density equals 4.7×10^{6} (molecule/Å^2). The relation between R_g and hydrodynamic radius can be obtained by combining the core-shell model density function and eq. (2.18),

$$R_g^2 = \frac{\int \rho(r) r^4 dr}{\int \rho(r) r^2 dr} \qquad (2.18)$$

$$\rho(\mathrm{r}) = \begin{cases} \Delta\rho_1 = \mathrm{SLD}_{\mathrm{core}} - \mathrm{SLD}_{\mathrm{solventl}} & 0 < r < R_1 \\ \Delta\rho_2 = \mathrm{SLD}_{\mathrm{shell}} - \mathrm{SLD}_{\mathrm{solvent}} & R_1 < r < R_2 \end{cases}$$

Thus we have equation for R_g and R

$$R_g = \sqrt{\frac{3}{5} \times \frac{(\Delta\rho_1 - \Delta\rho_2)R_1^5 + \Delta\rho_2 R_2^5}{(\Delta\rho_1 - \Delta\rho_2)R_1^3 + \Delta\rho_2 R_2^3}} \qquad (2.19)$$

There are four parameters affect the value of R_g. Because of the possibility of $\Delta\rho_1$ and $\Delta\rho_2$ being negative values, R_g may sometimes be larger than the hydrodynamic radius compared to $\sqrt{\frac{3}{5}}R$ when the molecule is a compact sphere. Comparison of R_g observed from Guinier plot, the R_g calculated from eq. (2.19) and the hydrodynamic radius from core-shell fitting result are in table 2-15, 2-16.

The calculated R_g are not exactly the same as the R_g observed from the Guinier plot. This results from the scattering length density difference between the core region and the shell region of the arborescent graft polymer which violate one of the assumptions for Guinier's law which is that the particle should have uniform density throughout the particle. However, the value of calculated R_g and the R_g observed from Guinier plots still follow the same trend.

The calculated R_g, is larger for generation 4 compared to generation 3 polymers under the same conditions. We can also conclude that R_g increases with increasing solvent quality by noting the smaller R_g in cyclohexane compared to toluene and

Table 2-15 Result of Hydrodynamic radius, Guinier radius of gyration and calculated radius of gyration for generation 3 AGP.

	G3		
	R_h	R_g	$R_{g\text{-}cal}$
Cyclohexane core match	240	229	199
THF core match	278	267	230
Toluene core match	277	265	229
Cyclohexane non match	245	247	213
THF non match	282	287	249
Toluene non match	276	289	249
Cyclohexane shell match	237	176	145
THF shell match	253	183	167
Toluene shell match	X	96	X

Table 2-16 Result of Hydrodynamic radius, Guinier radius of gyration and calculated radius of gyration for generation 4 AGP.

	G4		
	R_h	R_g From Guinier Plot	$R_{g\text{-}cal}$
Cyclohexane core match	378	358	328
THF core match	436	422	380
Toluene core match	430	417	374
Cyclohexane non match	378	422	383
THF non match	433	513	435
Toluene non match	430	507	440
Cyclohexane shell match	317	248	195
THF shell match	331	247	219
Toluene shell match	236	188	191

tetrahydrofuran. Toluene and tetrahydrofuran are good solvents while cyclohexane is a theta solvent for polystyrene. To understand the negative R_g observed from the

experimental scattering data, calculation of the scattering from the core-shell model at different solvent scattering length densities was performed. Parameters for the simulation were based on the fitting result of the G4 polymer in shell-match toluene mixtures except for the SLD_{core} and SLD_{shell} values. These SLD_{core} and SLD_{shell} values were set to be same as scatteringlength density of polystyrene and deuterated polystyrene respectively as the calculations. In figure 2-20, the calculated scattering shows that at certain values of the solvent scattering length density, the observed Guinier R_g is negative. Taking the core-shell model parameters as eq. (2.19), the equation for R_g as a function of $SLD_{solvent}$:

$$R_g = \sqrt{\frac{3}{5} \times \frac{4.54 \times 10^{12} - 7.48 \times 10^{11} \times SLD_{solvent}}{73347158 - 13312053 \times SLD_{solvent}}} \qquad (2.21)$$

We can predict that observed R_g will approach infinity when the denominator equals zero and R_g will approach zero when the numerator equals to zero. Figure 2-21 shows R_g calculated from eq. (2.21) as a function as $SLD_{solvent}$. When the $SLD_{solvent}$ is between 5.5×10^{-6} molecule/Å^2 and 6.05×10^{-6} molecule/Å^2, the R_g will be imaginary and the Guinier plot will have a positive slope as shown in figure 2-20.

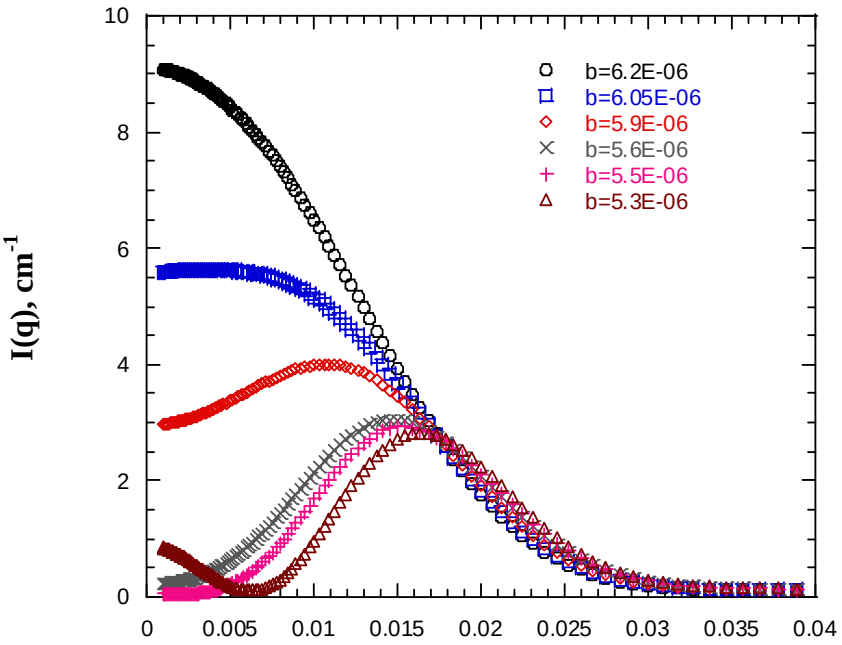

(a)

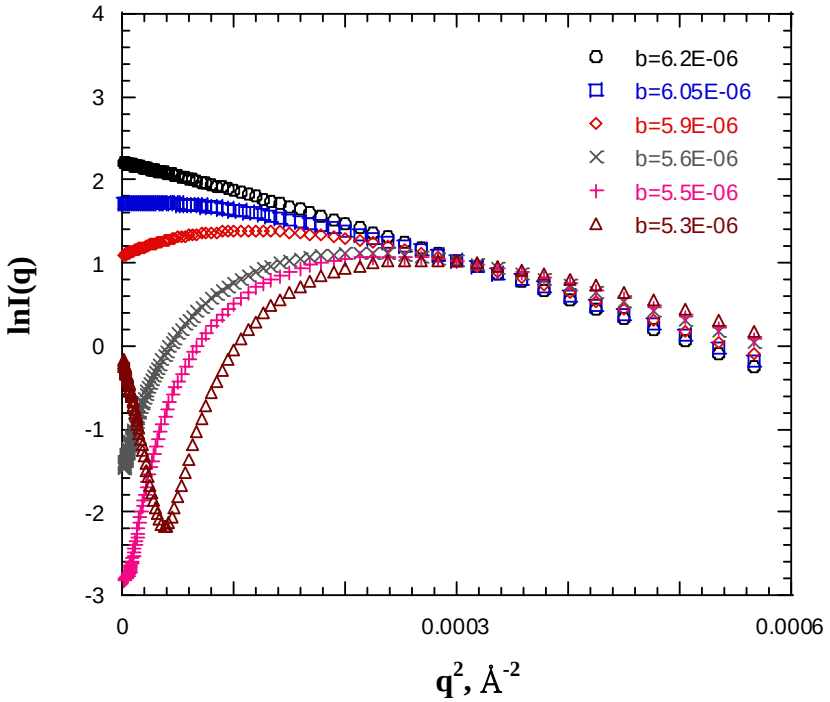

(b)

Figure 2-20 Scattering data and Guinier plot of simulation for core shell model under different scattering length density.

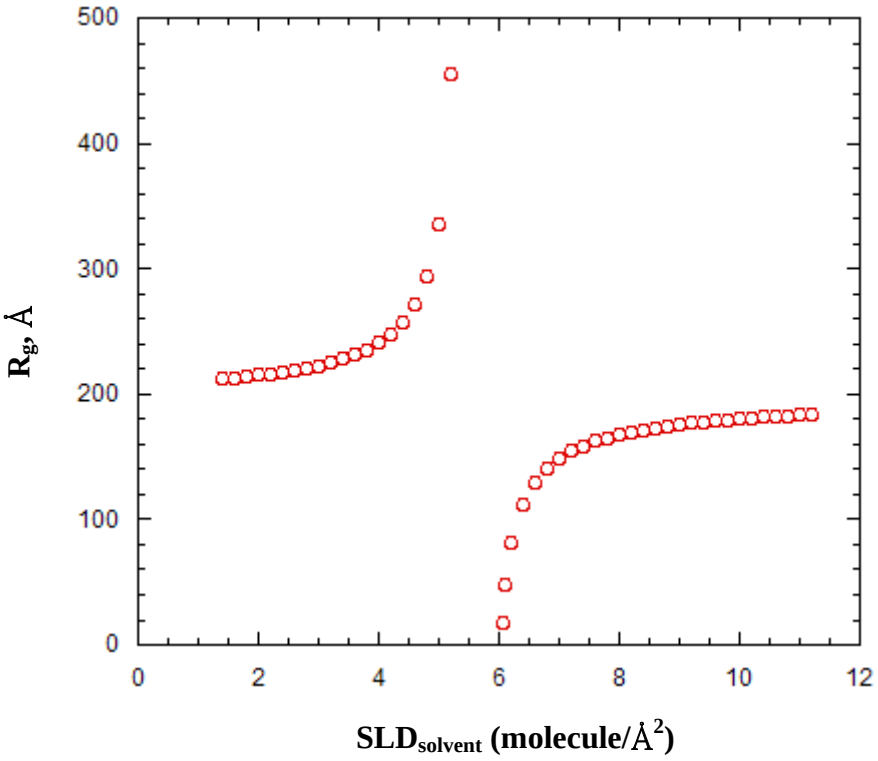

Figure 2-21 Calculated R_g as a function of solvent scattering length density.

2.5 CONCLUSIONs

Small-Angle neutron scattering has been used to measure generation 4 and generation 3 arborescent graft polymers in contrast matched solvents. A core-shell model with polydispersity has been used to fit the scattering data with good success. From the results, the volume fraction of solvent, polystyrene and deuterated polystyrene in the core and shell regions can be determined, and the mixing area of PS and deuterated PS due to random grafting reaction exists. However the thickness and its composition cannot be determined. It is also possible to calculate density profiles of generation 3 and generation 4 arborescent graft polymers in different solvents. The size of arborescent graft polymers increases with the increasing solvent quality.

The radius of gyration of the molecules dissolved in solvents with different scattering length densities were measured by Guinier plot. However it was found that the Guinier's law is not applicable in this case due to non-uniform density distribution of the molecule. The explicit equation to calculate the radius of gyration for core-shell model is found and has four parameters which are inner core radius, hydrodynamic radius, $SLD_{core} - SLD_{solvent}$, and $SLD_{shell} - SLD_{solvent}$. The equation is able to explain the observation of the imaginary radius of gyration under certain solvent scattering

length densities and a relatively large radius of gyration compared with the hydrodynamic radius. The radius of gyration increases from generation 3 to generation 4. The largest radius of gyration is found in non-match solvents and the smallest radius of gyration is observed in shell-match solvents. The radius of gyration is smaller for molecules in cyclohexane compared to toluene or tetrahydrofuran which indicates that the size of molecule is dominated by solvent quality.

Chapter 3 Future Work

The experimental scattering data of AGP in shell-match solvents were fit relatively well using the core-shell model (except the G3 polymer in deuterated toluene), although the interpretation of these fits is not clear. We had anticipated that these density profiles should behave like an unlabelled polystyrene AGP molecule of the corresponding generation. Efforts were made to fit these data with power law density function without polydispersity as given by eq. (3.1) [43]:

$$\rho(r) = 1 - \left(\frac{r}{R}\right)^{\alpha} \qquad (3.1)$$

where R corresponds to the hydrodynamic raidus. When α goes to infinity this model is equivalently to a hard sphere model. However, the fitting results were not good. In the future it would be interesting to determine the density profile of these arborescent graft polymers in shell-match solvents using a power law density function with polydispersity. It would also be interesting to analyze the density profiles of the

normal polystyrene arborescent graft polymer cores in different solvents. Comparing density profiles of the H/D labeled arborescent graft polymer and its polystyrene core would help to understand in more detail the interior structure. It would also be interesting to study density profiles of H/D labeled arborescent graft polymers in blends with different linear polymers and compare with density profiles of AGP in solvents.

Appendix I.a SANS Optics for Generation 4 Arborescent Graft Polymer in Solutions

- Wavelength of neutron: 8.09 Å
- Low q, q_{min} = 0.0009 $Å^{-1}$, q_{max} = 0.0229 $Å^{-1}$
- High q, q_{min} = 0.0061 $Å^{-1}$, q_{max} = 0.0637 $Å^{-1}$
- Wavelength Spread: $\Delta\lambda/\lambda = 0.1$
- Number of Guides: 6
- Source Aperture Diameter: 14 mm
- Sample Aperture Diameter: 15.9 mm
- Source-Sample Distance: 16.32 m
- Sample-Detector Distance: 15.3 m
- With lens.

Appendix I.b SANS Optics for Generation 3 Arborescent Graft Polymer in Solutions

- Wavelength of neutron: 6 Å
- Low q, q_{min} = 0.0035 $Å^{-1}$, q_{max} = 0.047 $Å^{-1}$
- High q, q_{min} = 0.008 $Å^{-1}$, q_{max} = 0.21 $Å^{-1}$
- Wavelength Spread: $\Delta\lambda/\lambda = 0.1$
- Number of Guides: 6
- Source Aperture Diameter: 50 mm
- Sample Aperture Diameter: 12.7 mm
- Source-Sample Distance: 11.67 m
- Sample-Detector Distance: 14.5 m
- With lens.

Appendix I.c SANS Optics for Generation 4 Arborescent Graft Polymer in Cyclohexane Solutions in H/D Ratios

- Wavelength of neutron: 8.09 Å
- Low q, q_{min} = 0.0015 $Å^{-1}$, q_{max} = 0.0229 $Å^{-1}$
- High q, q_{min} = 0.0061 $Å^{-1}$, q_{max} = 0.0637 $Å^{-1}$
- Wavelength Spread: $\Delta\lambda/\lambda = 0.1$
- Number of Guides: 0
- Source Aperture Diameter: 14 mm
- Sample Aperture Diameter: 12.7 mm
- Source-Sample Distance: 16.32 m
- Sample-Detector Distance: 15.3 m
- With lens.

GLOSSARY OF SYMBOLS

b_i	Neutron scattering length for species *i* in the mixture.
F	Form factor.
$F_s(q)$	Single particle form factor.
$F_0(q)$	Hard sphere form factor.
f(r)	Normalized probability.
G	Generation number of arborescent graft polymer.
I(q)	Scattered intensity.
$\mathbf{k_i}$	Incident wave vector.
$\mathbf{k_s}$	Scattered wave vector.
k_n	Contrast factor for neutrons.
M_w	Weight average molecular weight.
N_a	Avogadro's number.
P(q)	Single particle form factor.
q	Scattering Vector.
q	Magnitude of the scattering wave vector.
R	Hydrodynamic radius.

R_g Radius of gyration.

$\bar{r}$ Mean particle size.

$S(q)$ Structure factor.

V Total volume of the particle.

Greek Letters

ϕ Concentration of the scatterers.

ϕ_{PS}^{core} Volume fraction of polystyrene in the core region of the molecule.

ϕ_{dPS}^{core} Volume fraction of deuterated polystyrene in the core region of the molecule.

$\phi_{solvent}^{core}$ Volume fraction of solvent in the core region of the molecule.

λ Wavelength of neutrons.

v_i Specific volume of species *i*.

ρ(r) Density profile.

σ^2 Variance of the distribution.

REFERENCES

1. G. Odian, *Principles of Polymerization*, John & Sons, Inc., 1991.

2. P. G. de Gennes, *Scaling Concepts in Polymer Physics*, Cornell University, New York, 1979.

3. R. H. Boyd and P. J. Phllips, *The Science of Polymer Molecules*, Cambridge University Press, New York, 1993.

4. D. A. Tomalia, D. M. Hedstrand, and L. R. Wilson, *Encyclopedia of Polymer Science and Engineering*, Index Volume, John Wiley & Sons, New York, 1990.

5. T. H. Mourey, S. R. Turner, M. Rubinstein, J. M. Frechet, C. J. Hawker, and K. L. Wooley, *Macromolecules*, **25**, 2401 (1992).

6. S. R. Turner, B. I. Voit, and T. H. Mourey, *Macromolecules*, **26**, 4617 (1993).

7. M. Gauthier, W. Li, and L. Tichagwa, *Polymer*, **38**, 6363 (1997).

8. D. A. Tomalia, H. Baker, J. Dewald, M. Hall, G. Kalos, S. Martin, J. Roeck, J. Ryder, and P. Smith, *Polymer Journal*, **17**, 117 (1985).

9. W. Worthy, *Chemical Emgineering News*, **66**, 19 (1998).

10. D. A. Tomalia, A. M. Naylor, and W. A. Goddard, *Angew. Chem. Int. Ed. Engl.*, **29**, 138 (1990).

11. Y. H. Kim and O. W. Webster, *J. Am. Chem. Soc.*, **112**, 4592 (1990).

12. M. Gauthier and M. Moeller, *Macromolecules*, **24**, 4548 (1991).

13. M. Gauthier, M. Moeller, and W. Burchard, *Macromol. Symp.*, **77**, 43 (1994).

14. M. Gauthier, L. Tichagwa, J. S. Downey, and S. Gao, *Macromolecules*, **29**, 519 (1996).

15. S. S. Sheiko, M. Gauthier, and M. Moeller, *Macromolecules*, **30**, 2343 (1997).

16. R. S. Frank, G. Merkle, and M. Gauthier, *Macromolecules*, **30**, 5397 (1997).

17. M. Gauthier, J. Chung, L. Choi, and T. T. Nguyen, *J. Phys. Chem B*, **102**, 3138 (1998).

18. T. J. Prosa, B. J. Bauer, E. J. Amis, D. A. Tomalia, and R. Scherrenberg, *J.*

Polymer Science, **35**, 2914, (1997).

19. L. Lue and J. M. Prausnitz, *Macromolecules*, **30**, 6650 (1997).

20. D. Boris and M. Rubinstein, *Macromolecules*, **29**, 7251 (1996).

21. J. Li, M. Gauthier, S. J. Teertstra, H. Xu, S.S. Sheiki, *Macromolecules*, 37, 795 (2004).

22. M. Gauthier, J LI, J. Dockendorff, *Macromolecules*, 36, 2642(2003).

23. J li, M Gauthier, *Macromolecules*, 34,8918(2001).

24. T. J. Prosa, B. J. Bauer, E. J. Amis, D. A. Tomalia, R. Scherrenberg, *Journal of Polymer Science*, 35, 2913(1997)

25. J. S. Higgins, H. C. Benoit, *Polymers and Neutron Scattering*, Oxford Science Publications : New York, 1994

26. N. Dingenouts, M Ballauff, *Langmuir*,15, 3283(1999)

27. P. G. de Gennes and H. Hervet, *J. Physiol. Lett.*, **44**, L351 (1983).

28. R. L. Lascanec and K. Muthukumar, *Macromolecules*, **23**, 2280 (1990).

29. M. L. Mansfield and L. I. Klushin, *Macromolecules*, **26**, 4262 (1993).

30. M. L. Mansfield, *Polymer*, **35**, 1872, (1994).

31. M. Murat and G. S. Grest, *Macromolecules*, **29**, 1278 (1996).

32. A. M. Naylor and W. A. Goddard, *Polym. Prepr.*, **29**, 215, (1988).

33. A. M. Naylor, W. A. Goddard, G. Keifer, and D. A. Tomalia, *J. Am. Chem. Soc.*, **111**, 2339, (1989).

34. S. Stechemesser and W. Eimer, *Macromolecules*, **30**, 2204 (1997).

35. A. Topp, B. J. Bauer, D. A. Tomalia, and E. J. Amis Submitted to *Macromolecules*.

36. T. J. Prosa, B. J. Bauer, and E. J. Amis To be submitted.

37. *NG3 and NG7 30-meter SANS Instruments Data Acquistion Manual*, National Institute of Standards and Technology Cold Neutron Research Facility, 1996.

38. C. J. Glinka, J. G. Barker, B. Hammouda, S. Krueger, J. J. Moyer, and W. J. Orts, *J. Appl. Cryst.*, **31**, 430 (1998).

39. R.H. Boyd, P.J. Phillips, *The Science of Polymer Molecules*, Cambridge University Press, New York, 1996

40. Lord Rayleigh *Proc. R. Soc. London, Ser.* A, 90, 219, 1914

41. J. B. Hayter in *Physics of Amphiphiles--Micelles, Vesicles, and Microemulsions*, Eds.V. DeGiorgio; M. Corti, pp. 59-93,1983.

42. http://www.ncnr.nist.gov/programs/sans/manuals/data_anal.html

43. S. Choi, R. M. Briber, B. J. Bauer, A. Topp, M. Gauthier, L. Tichagwa, *Macromolecules*, **32**, 7879 (1999)